Unravelling an extended quark sector through multiple Higgs production?

S. Dawson, E. Furlan, and I. Lewis

Unravelling an extended quark sector through multiple Higgs production?

S. Dawson, E. Furlan, and I. Lewis

Department of Physics, Brookhaven National Laboratory, Upton, New York, 11973

Abstract

In many new physics scenarios, the particle content of the Standard Model is extended and the Higgs couplings are modified, sometimes without affecting single Higgs production. We analyse two models with additional quarks. In these models, we compute double Higgs production from gluon fusion exactly at leading-order, and present analytical results in the heavy-quark mass approximation. The experimental bounds from precision electroweak measurements and from the measured rate of single Higgs production combine to give significant restrictions for the allowed deviation of the double Higgs production rate from the Standard Model prediction as well as on the branching ratio for the Higgs decay into photons. The two models analysed eventually present a similar Higgs phenomenology as the Standard Model. We connect this result to the magnitude of the dimension six operators contributing to the gluon-fusion Higgs production.

I. INTRODUCTION

The search for the source of electroweak symmetry breaking has dominated particle theorist's efforts for decades. Now that a particle with many of the right properties to be the Higgs boson of the Standard Model has been discovered [1, 2], the efforts turn to understanding the properties of this particle. In the Standard Model, the couplings of the Higgs boson to fermions, gauge bosons, and to itself are firm predictions of the model. In models with new physics, however, these couplings can be different.

The dominant production mechanism for a Higgs boson is gluon fusion, which is sensitive to many types of new physics. The simplest possibility is for new heavy colored scalars [3, 4] and/or fermions [5–15] to contribute to Higgs production. However, since the observed Higgs candidate particle is produced at roughly the Standard Model rate, extensions of the Higgs sector beyond the Standard Model are extremely constrained. For example, a model with a sequential fourth generation of chiral fermions predicts large deviations in the Higgs rates [16–20] and is excluded by the limits on Higgs production for any Higgs mass below around 600 GeV [21, 22]. The properties of these potential new colored particles are further limited by precision electroweak measurements. Models in which the Higgs boson is composite [23–34], along with models which generate new higher dimension effective operators involving the Higgs boson and gluons [35, 36], can also induce a single Higgs production rate different from that of the Standard Model. Untangling the source of possible deviations from the Standard Model by measuring the production and decay rates of the Higgs boson will be quite difficult in models where there are only small differences from the Standard Model predictions.

In this paper, we examine the extent to which the gluon fusion production of two Higgs bosons can have a rate very different from that predicted by the Standard Model [37, 38], given the restrictions from electroweak precision physics and from single Higgs production. The observation of double Higgs production via gluon fusion is important in order to measure the cubic self coupling of the Higgs boson [39, 40]. In the Standard Model, the rate is small, although the $\mathcal{O}(\alpha_s^3)$ radiative corrections are known in the infinite top quark mass limit and are large [41, 42]. For a 125 GeV Higgs particle, the most likely channel for HH exploration is $gg \rightarrow HH \rightarrow b\bar{b}\gamma\gamma$ [43], where studies have estimated that the LHC at full energy will be sensitive to this process with around 600 fb^{-1}. Using jet substructure techniques, the

$HH \to b\bar{b}W^+W^-$ and $HH \to b\bar{b}\tau^+\tau^-$ channels may be available with about 600 fb^{-1}[44] and 1000 fb^{-1}[40]. This is clearly not physics which will be done during the early phase of LHC operations, unless the rate is significantly larger than in the Standard Model [45].

Double Higgs production can further be studied through vector boson fusion, which is also sensitive to the three Higgs self coupling [46]. Vector boson fusion production of two Higgs bosons can be affected by new operators involving the W and Z gauge bosons and the Higgs, but is not sensitive to the new colored particles which contribute to the gluon fusion process. Hence the two production mechanisms can provide complementary information.

Double Higgs production from gluon fusion first occurs at one loop and is therefore potentially modified by the same new heavy colored particles which contribute to single Higgs production. However, as pointed out in Ref. [36], single and double Higgs production are sensitive to different higher dimension effective operators and in principle, the single Higgs production rate could be Standard Model like, while the double Higgs production could be highly suppressed or enhanced. Here, we consider the effects of both heavy vector-like and chiral colored fermions on the single and double Higgs production rates, and the interplay between them. We will not consider models with extended Higgs sectors, or with higher dimension non-renormalizable operators.

For single Higgs production, it is useful to analyze the effects of non-Standard Model colored particles using a low energy theorem [47]. The theorem can be formulated using the background field method in terms of the traces of the mass matrices of colored objects, which eliminates the need to diagonalize complicated mass matrices [48]. The low energy theorem can be extended to double Higgs production, where new features arise [34]. In models with extended fermion sectors (for example, in little Higgs models [49–55]) there are contributions to double Higgs production containing more than one flavor of fermion [56]. These diagrams contain axial couplings to the Higgs boson which are non-diagonal in the fermion states and we demonstrate how these effects can be included using a low energy theorem. Low energy theorems are extremely useful for single Higgs production and generally give estimates of the total cross section which are quite accurate. For double Higgs production, however, the low energy theorems provide an estimate of the total rate which typically disagrees with the exact rate by 50% or more. The low energy theorem does not reproduce kinematic distributions accurately, but instead predicts high energy tails which are not present in the full theory [57].
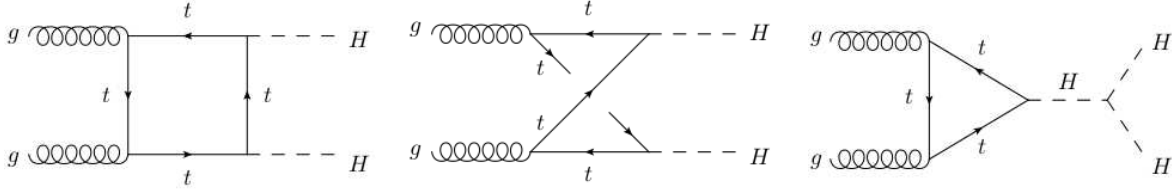
FIG. 1: Feynman diagrams for $gg \to HH$ in the Standard Model.

In this paper, we study the effects of heavy colored fermions on the gluon fusion double Higgs production rate and show that agreement with single Higgs production requires the double Higgs rate to be close to that of the Standard Model. We demonstrate how this can be understood in terms of the effective operator approach of Ref. [36] and discuss the limitations of the low energy theorem for $gg \to HH$. Interestingly, composite Higgs models and little Higgs models receive potentially large corrections to the $gg \to HH$ process from the non-renormalizable operator $t\bar{t}HH$. The observation of such a large effect would be a "smoking gun" signal for such models [33, 34, 45].

II. DOUBLE HIGGS PRODUCTION

1. The Standard Model

In the Standard Model, double Higgs production from a gluon-gluon initial state arises from the Feynman diagrams shown in Fig. 1. The result is sensitive to new colored objects (fermions or scalars) in the loops and to the Higgs trilinear self-coupling. The amplitude for $g^{a,\mu}(p_1)g^{b,\nu}(p_2) \to H(p_3)H(p_4)$ is

$$A_{ab}^{\mu\nu} = \frac{\alpha_s}{8\pi v^2}\delta_{ab}\left[P_1^{\mu\nu}(p_1,p_2)F_1(s,t,u,m_t^2) + P_2^{\mu\nu}(p_1,p_2,p_3)F_2(s,t,u,m_t^2)\right] , \qquad (1)$$

where P_1 and P_2 are the orthogonal projectors onto the spin-0 and spin-2 states respectively,

$$
\begin{aligned}
P_1^{\mu\nu}(p_1,p_2) &= g^{\mu\nu} - \frac{p_1^\nu p_2^\mu}{p_1 \cdot p_2} , \\
P_2^{\mu\nu}(p_1,p_2,p_3) &= g^{\mu\nu} + \frac{2}{sp_T^2}\left(m_H^2 p_1^\nu p_2^\mu - 2p_1{\cdot}p_3\,p_2^\mu p_3^\nu - 2p_2{\cdot}p_3\,p_1^\nu p_3^\mu + s\,p_3^\mu p_3^\nu\right) ,
\end{aligned} \qquad (2)
$$

s, t, and u are the partonic Mandelstam variables,

$$s = (p_1 + p_2)^2 , \quad t = (p_1 - p_3)^2 , \quad u = (p_2 - p_3)^2 , \qquad (3)$$

4

p_T is the transverse momentum of the Higgs particle,

$$p_T^2 = \frac{ut - m_H^4}{s} , \tag{4}$$

and $v = (\sqrt{2}G_F)^{-1/2} = 246$ GeV. The functions F_1 and F_2 are known analytically [37, 38]. Finally, the partonic cross section is given by

$$\frac{d\hat{\sigma}(gg \to HH)}{dt} = \frac{\alpha_s^2}{2^{15}\pi^3 v^4} \frac{|F_1(s,t,u,m_t^2)|^2 + |F_2(s,t,u,m_t^2)|^2}{s^2} , \tag{5}$$

where we included the factor of $\frac{1}{2}$ for identical particles in the final state.

In the Standard Model, the chiral fermions are

$$\psi_L^i = \begin{pmatrix} u_L^i \\ d_L^i \end{pmatrix} , \quad u_R^i, \, d_R^i , \tag{6}$$

where $i = 1, 2, 3$ is a generation index and the Lagrangian describing the quark masses is

$$-\mathcal{L}_M^{SM} = \sum_i \lambda_i^d \overline{\psi}_L^i \Phi d_R^i + \lambda_i^u \overline{\psi}_L^i \tilde{\Phi} u_R^i + \text{h.c.} . \tag{7}$$

Here $\Phi = (\phi^+, \phi^0)^T$ is the Higgs doublet, $\tilde{\Phi} = i\sigma_2 \Phi^*$ and $\phi^0 = \frac{v+H}{\sqrt{2}}$. Note that in the Standard Model the Higgs couplings $\lambda_i^{u,d}$ are purely scalar. In the following we will focus on the third generation quarks and use the standard notation $u^3 = t$, $d^3 = b$, with $\lambda_3^d \equiv \lambda_1$ and $\lambda_3^u \equiv \lambda_2$.

In the Standard Model, the dominant contributions come from top quark loops. Analytic expansion of the amplitudes in the limit $m_t^2 >> s$ yields the leading terms

$$\begin{aligned}
F_1(s,t,u,m_t^2) &\equiv F_1^{tri}(s,t,u,m_t^2) + F_1^{box}(s,t,u,m_t^2) , \\
F_1^{tri}(s,t,u,m_t^2) &= \frac{4m_H^2}{s - m_H^2} s \left\{ 1 + \frac{7}{120}\frac{s}{m_t^2} + \frac{1}{168}\frac{s^2}{m_t^4} + \mathcal{O}\left(\frac{s^3}{m_t^6}\right) \right\} , \\
F_1^{box}(s,t,u,m_t^2) &= -\frac{4}{3}s \left\{ 1 + \frac{7}{20}\frac{m_H^2}{m_t^2} + \frac{90m_H^4 - 28m_H^2 s + 12s^2 - 13p_T^2 s}{840m_t^4} + \mathcal{O}\left(\frac{s^3}{m_t^6}\right) \right\} ; \\
F_2(s,t,u,m_t^2) &= -\frac{11}{45}s\frac{p_T^2}{m_t^2} \left\{ 1 + \frac{62m_H^2 - 5s}{154m_t^2} + \mathcal{O}\left(\frac{s^2}{m_t^4}\right) \right\} .
\end{aligned} \tag{8}$$

The leading terms in the inverse top mass expansion of Eq. 8 are called the "low energy theorem" result and give the m_t-independent amplitudes [37, 38]

$$\begin{aligned}
F_1(s,t,u,m_t^2) \mid_{LET} &\to \left(-\frac{4}{3} + \frac{4m_H^2}{s - m_H^2} \right) s , \\
F_2(s,t,u,m_t^2) \mid_{LET} &\to 0 .
\end{aligned} \tag{9}$$

5

From Eq. 8, we can clearly see that the triangle diagram has no angular dependence and only makes an s-wave contribution. This result is expected since the triangle diagram has a triple-scalar coupling, which has no angular momentum dependence. For the box diagrams, at the lowest order in F_2^{box} there is angular momentum dependence reflected in p_T^2, which is expected from the spin-2 initial state and spin-0 final state. At $\mathcal{O}(m_t^{-4})$ in F_1^{box} there is also an angular momentum dependent piece proportional to p_T^2. Since the initial and final states for the F_1 contribution are both spin-0, this is a somewhat surprising result. To gain insight into the angular dependence of F_1^{box} and further insight into F_2^{box}, the functions can be decomposed into Wigner d-functions, $d^j_{s_i,s_f}$, where j is the total angular momentum and s_i (s_f) is in the initial (final) state spin:

$$
\begin{aligned}
F_1^{box}(s,t,u,m_t^2) &= -\frac{4}{3}s\left[\left(1+\frac{7}{20}\frac{m_H^2}{m_t^2}+\frac{540m_H^4-116m_H^2s+59s^2}{5040m_t^4}\right)d^0_{0,0}(\theta)\right.\\
&\quad\left.+\frac{13s^2-52m_H^2s}{5040m_t^4}d^2_{0,0}(\theta)+\mathcal{O}\left(\frac{s^3}{m_t^6}\right)\right],\\
F_2^{box}(s,t,u,m_t^2) &= -\frac{11}{45}s\frac{s-4m_H^2}{\sqrt{6}m_t^2}\left[1+\frac{62m_H^2-5s}{154m_t^2}+\mathcal{O}\left(\frac{s^2}{m_t^4}\right)\right]d^2_{2,0}(\theta).
\end{aligned}
\tag{10}
$$

Here θ is the angle between an initial state gluon and final state Higgs,

$$
t = m_H^2 - \frac{s}{4}\left(1-\beta\cos\theta\right) \quad\text{and}\quad \beta = \sqrt{1-\frac{4m_H^2}{s}}.
\tag{11}
$$

In F_1^{box}, we can see the expected spin-0 s-wave component, $d^0_{0,0}$, and an additional spin-0 d-wave component, $d^2_{0,0}$, at $\mathcal{O}(m_t^{-4})$. The s-wave and d-wave components are orthogonal. Hence any angular independent observables, such as total cross section and invariant mass distribution, are independent of the p_T^2 component of F_1^{box} up to $\mathcal{O}(m_t^{-8})$. Finally, F_2^{box} is wholly dependent on the initial state spin-2 d-wave function $d^2_{2,0}$, as expected from Eq. 1.

In Fig. 2, we compare the total cross section for double Higgs production at different orders in the large mass expansion against the exact result[1], as a function of the center of mass energy in pp collisions. We use the CT10 NLO PDF set [58] and run the strong coupling constant through NLO from its value $\alpha_s(m_Z) = 0.118$. We fix $m_t = 173$ GeV and $m_b = 4.6$ GeV. The low energy theorem results are quite sensitive to the scale choice, and typically reproduce the exact results to within roughly 50% error. This "agreement" between the infinite mass approximation (LET) and the exact result is not improved by the inclusion

---

[1] The exact result always includes the contributions from both the top and bottom quarks.
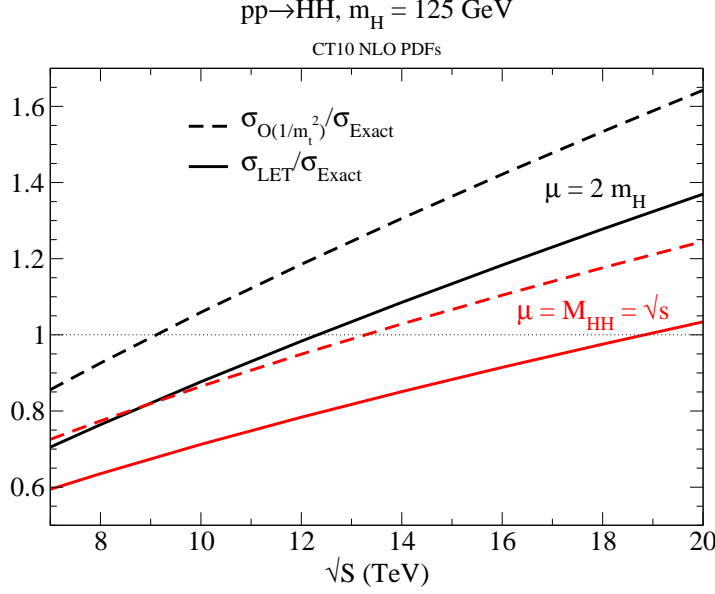
FIG. 2: Double Higgs production cross section as a function of the hadronic center of mass energy $\sqrt{S}$ in the infinite top mass approximation, LET, (solid lines) and retaining the $\mathcal{O}\left(\frac{s}{m_t^2}\right)$ corrections (dashed lines), normalized to the exact result. The black (red) curves choose as the renormalization and factorization scales $\mu = 2m_H$ ($\mu = M_{HH} = \sqrt{s}$).

of higher orders in the large mass expansion. In single Higgs production, the reliability of the infinite mass approximation has been investigated through NNLO [59–62]. Because of the shape of the gluon parton luminosity, which peaks at large values of $x = m_H^2/s$ and decreases rapidly, the largest contribution to the hadronic single Higgs cross section comes from the region below the top quark threshold, $s < 4m_t^2$, where the large top mass approximation holds. As a consequence, finite mass corrections to single Higgs production have an effect of less than 1%. On the other hand, for double Higgs production the partonic energy is always $s > 4m_H^2$ and the condition for validity of the low energy theorem, $s \ll 4m_t^2$, is typically not satisfied.

Fig. 3 shows the sensitivity of the results to the choice of the PDF sets. The exact result has a small sensitivity to the choice of LO vs NLO PDFs. However, the infinite mass limit (LET) of the result is quite sensitive to the choice of PDFs. Including higher order terms in the top mass expansion does not reduce this sensitivity to the choice of PDFs.

The inadequacy of the infinite mass approximation for double Higgs production becomes even more apparent when looking at kinematic distributions [57]. Consider for example the
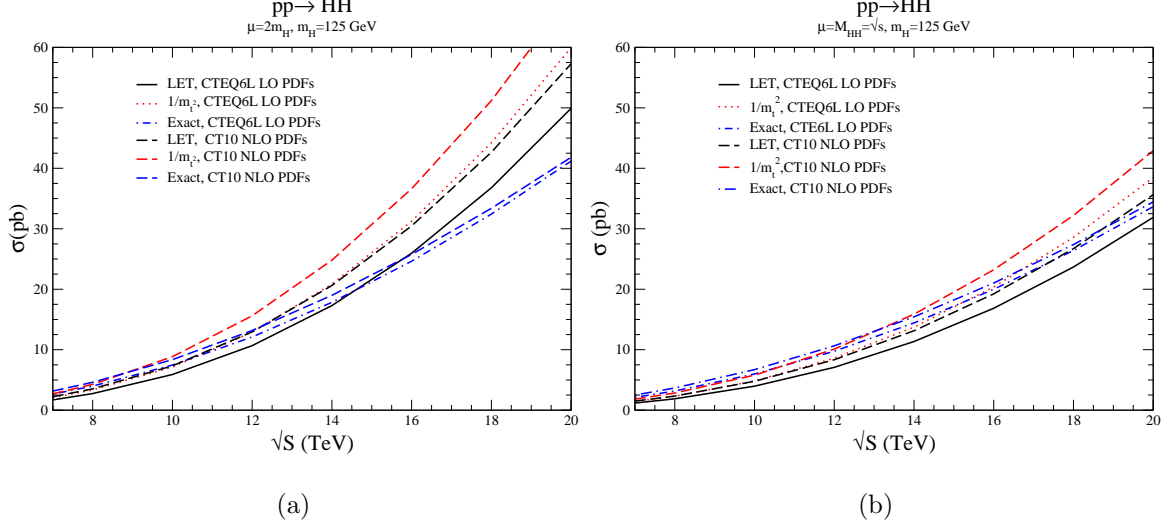
FIG. 3: Total cross sections for HH production using CTEQ6L LO PDFS and CT10 NLO PDFs. The renormalization/factorization scale is $\mu = 2m_H$ in (a) and $\mu = M_{HH} = \sqrt{s}$ in (b). For all curves, α_s is evaluated at NLO.

invariant mass of the HH system,

$$
\frac{d\sigma(pp \to HH)}{dM_{HH}} = \frac{2M_{HH}}{S}\hat{\sigma}(gg \to HH)\frac{d\mathcal{L}_{gg}}{d\tau} \quad ,
$$
$$
\frac{d\mathcal{L}_{gg}}{d\tau} = \int_\tau^1 \frac{dx}{x}g(x,\mu_F)g\left(\frac{\tau}{x},\mu_F\right) , \tag{12}
$$

where S is the hadronic center of mass energy squared, $M_{HH} = \sqrt{s}$, and $\tau = \frac{s}{S}$. In Fig. 4 we analyse the impact of the finite mass corrections to the invariant mass distribution at
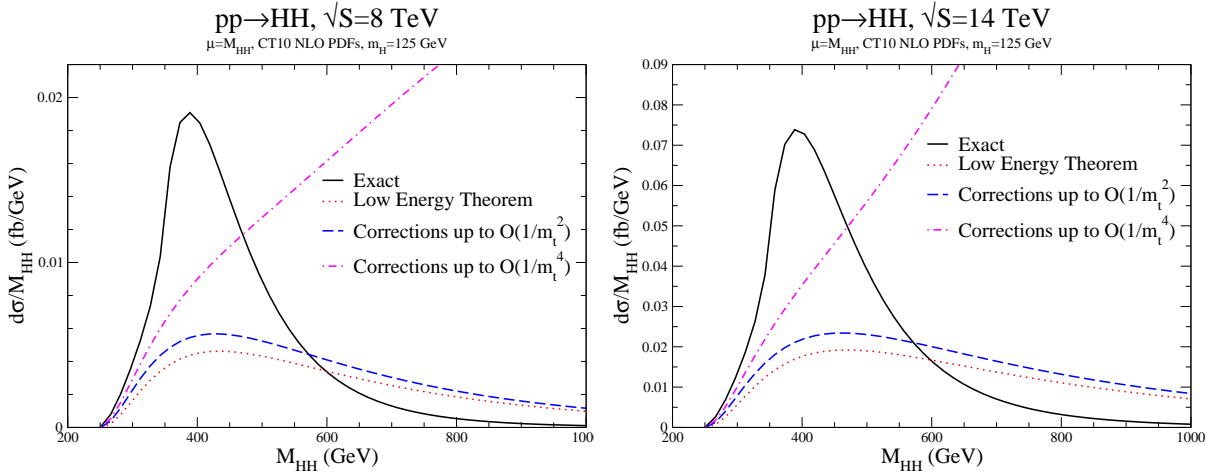

FIG. 4: Invariant mass distributions for Higgs pair-production at $\sqrt{S} = 8$ TeV and $\sqrt{S} = 14$ TeV, for terms in the large mass expansion up to $\mathcal{O}(m_t^{-4})$ (Eq. 8) and with the full mass dependence.
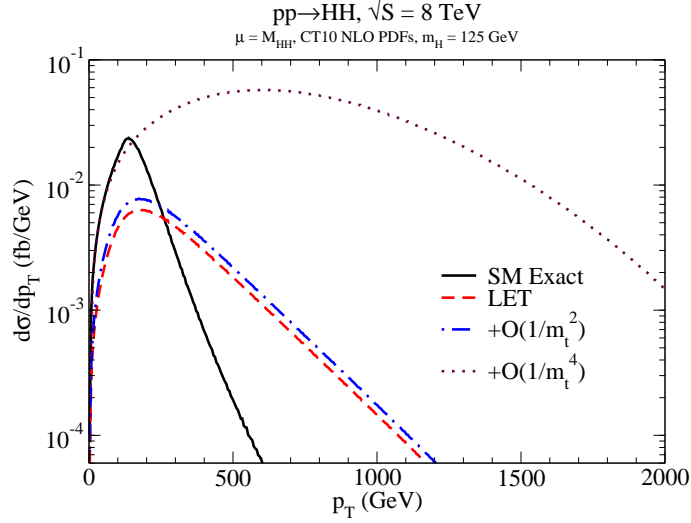
FIG. 5: Transverse momentum distribution for double Higgs production cross section. The Standard Model exact result, the LET and the heavy top mass approximations up to $\mathcal{O}(m_t^{-4})$ are shown. We choose as the renormalization and factorization scales $\mu = M_{HH} = \sqrt{s}$ and use the CT10 NLO PDFs.

the $\sqrt{S} = 8$ TeV and $\sqrt{S} = 14$ TeV LHC. The inclusion of the $\mathcal{O}(m_t^{-2})$ corrections does not significantly improve the low energy theorem results. The m_t^{-4} terms fail entirely in reproducing the exact distribution, in particular at large values of M_{HH}. Similar features are observed in the p_T spectrum shown in Fig. 5. Even for very small $p_T \ll m_t$, the infinite mass spectrum does not reproduce the distribution accurately, although the transverse momentum distribution is well described when including the $\mathcal{O}(m_t^{-4})$ terms. However, for $p_T > m_t$, the results from the heavy mass expansion drastically fail to approximate the exact distributions. A similar behaviour has been observed for the differential cross section $d\sigma/dp_T$ in higher order corrections to single Higgs production [63].

2. Non-Standard Model bottom quark Yukawa coupling

We briefly discuss the role of the bottom quark loops which are omitted when using the low energy theorems. In Fig. 6, we show the exact kinematic distribution for double Higgs production in the Standard Model, along with the result of the low energy theorem. The bottom quark contribution is negative but negligible in the Standard Model ($C_b = \frac{y_{bb}}{m_b} = 1$ is
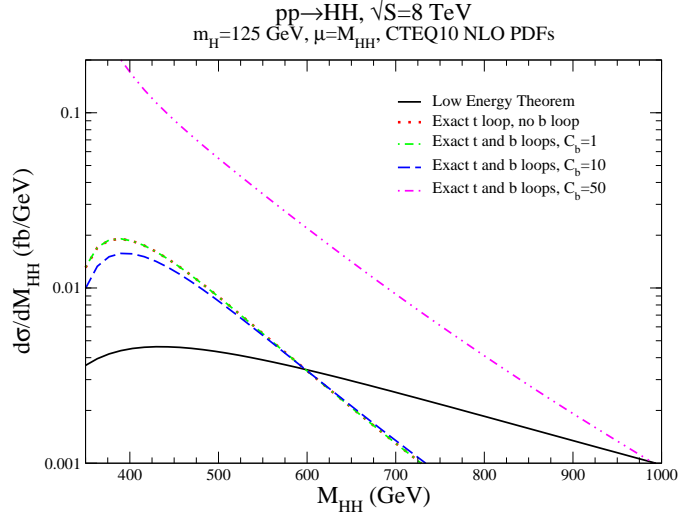
FIG. 6: Invariant mass distribution for Higgs pair production at $\sqrt{S} = 8$ TeV, in the infinite top mass approximation (solid black), with the full dependence on m_t, but no b quark contribution, (red dotted) and including bottom-quark effects for increasing values of the Higgs-bottom quark Yukawa coupling (dashed lines).

a rescaling factor of the bottom Yukawa coupling y_{bb} with respect to the Standard Model). The result of the destructive interference between the top and bottom quark loops remains small even when the bottom Yukawa is scaled up by a factor of 10. Only enhancements by factors as large as 50 cause the bottom loops to dominate and give significant deviations. In the Standard Model (with CT10 NLO PDFs and $\mu = M_{HH}$), at $\sqrt{S} = 8$ TeV, the infinite mass approximation for the two Higgs cross section is about 70% of the exact two Higgs cross section. This remains roughly true if C_b is increased to ~ 10. However, if the b quark Yukawa coupling is increased by a factor of 50, this ratio goes to 9, and the low energy theorem is wildly inaccurate.

3. Additional heavy quarks

A simple extension of the Standard Model with additional quarks of charge $\frac{2}{3}$ which can mix with the Standard Model like top occurs in many new physics scenarios, for example little Higgs [49–52, 64] and composite Higgs [23–26, 28–34] models. There can also be new heavy charge $-\frac{1}{3}$ quarks [65, 66] and the formulae in this section apply to both cases. We
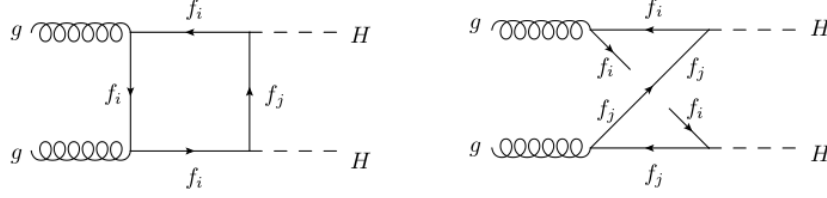
FIG. 7: Additional Feynman diagrams contributing to $gg \to HH$ in models with new heavy quarks coupling to the Higgs boson through non-diagonal Yukawa interactions.

will take the new quarks to be in the fundamental representation of the color group. For an overview of the latest lower bounds on the masses of the additional quarks, see for example Refs. [5, 67]. Note however that the experimental analyses always assume the new quarks to decay entirely either through W or though Z. This is not the case in our models, and the experimental limits are therefore weakened [6, 68, 69].

In addition to the diagrams of Fig. 1, where any of the heavy quarks can be running in the loop, the double Higgs production receives contributions also from the mixed diagrams with two different quarks of Fig. 7. The mass terms and the interactions with a Higgs boson of a pair of mass eigenstate quarks f_i, f_j (of the same charge) are

$$
\begin{aligned}
-\mathcal{L}_H &= \sum_{i,j} \overline{f}_{i,L} \left(m_i \delta_{ij} + \frac{y_{ij}}{v} H \right) f_{j,R} + \text{h.c.} \\
&= \sum_{i,j} \overline{f}_i \left(m_i \delta_{ij} + \frac{Y_{ij} + \gamma_5 A_{ij}}{v} H \right) f_j ,
\end{aligned}
\tag{13}
$$

with

$$
Y_{ij} = \frac{y_{ij} + y_{ji}^*}{2} \quad , \quad A_{ij} = \frac{y_{ij} - y_{ji}^*}{2} .
\tag{14}
$$

We consider real couplings. Therefore $Y_{ij} = Y_{ji}$ and $A_{ij} = -A_{ji}$, and only the terms involving two different quarks f_i and f_j contain pseudo-scalar couplings,

$$
-\mathcal{L}_H = \sum_i \frac{Y_{ii}}{v} \overline{f}_i H f_i + \sum_{i \neq j} \overline{f}_i \left(\frac{Y_{ij} + \gamma_5 A_{ij}}{v} \right) H f_j .
\tag{15}
$$

In the Standard Model $Y_{ii} = m_i$ and $A_{ij} = 0$.

For arbitrary masses m_i and m_j,

$$
\begin{aligned}
F_1^{tri}(s,t,u,m_i^2,m_j^2) &= \frac{Y_{ii}}{m_i} F_1^{tri}(s,t,u,m_i^2) + \frac{Y_{jj}}{m_j} F_1^{tri}(s,t,u,m_j^2) \\
&= \frac{4m_H^2}{s - m_H^2} s \operatorname{Tr} \left(y \mathcal{M}^{-1} \right) + \mathcal{O}\left(\frac{s^2}{m^4} \right),
\end{aligned}
\tag{16}
$$

11

where y and $\mathcal{M}$ are the Yukawa and the heavy quark mass matrices from Eq. 13. For the box topologies, the leading terms in the large quark mass expansion are

$$
\begin{aligned}
F_1^{box}(s,t,u,m_i,m_j) &= -\frac{4}{3}s\left\{\frac{Y_{ii}^2}{m_i^2}+\frac{Y_{jj}^2}{m_j^2}+\frac{2\left(Y_{ij}^2-A_{ij}^2\right)}{m_i m_j}\right\}+\mathcal{O}\left(\frac{s^2}{m^4}\right) \\
&= -\frac{4}{3}s\,\mathrm{Tr}\left(y\mathcal{M}^{-1}y\mathcal{M}^{-1}\right)+\mathcal{O}\left(\frac{s^2}{m^4}\right), \\
F_2(s,t,u,m_i,m_j) &= \mathcal{O}\left(\frac{s^2}{m^4}\right).
\end{aligned}
\tag{17}
$$

The relative minus sign between the vector and axial contributions comes from Eq. 14.

Although the leading terms of the triangle and box diagrams were calculated in the diagonal mass basis, the cyclicity of the trace and the fact that both $\mathcal{M}$ and y rotate according to the same unitary transformations allow one to cast the results in Eqs. 16 and 17 into a basis independent form. Hence the Yukawa and mass matrices can be evaluated both in the mass basis, where $\mathcal{M}$ is diagonal, and in the current basis. In the current basis, $y = \frac{\partial \mathcal{M}}{\partial v}$. The infinite mass limit of both the triangle and box diagrams can also be obtained via the low energy theorems [47, 48].

In our calculations in Sections III A and III B, we retain the full dependence of the leading order amplitude on the quark masses. However, for small mass splitting $\delta \equiv m_j^2 - m_i^2$ the sub-leading terms have a simple and useful form,

$$
\begin{aligned}
F_1^{box}(s,t,u,m_i^2,\delta) &= \frac{Y_{ii}^2+Y_{jj}^2+2Y_{ij}^2}{m_i^2}F_1^{box}(s,t,u,m_i^2)+\frac{4}{3}s\frac{Y_{jj}^2+Y_{ij}^2}{m_i^2}\frac{\delta}{m_i^2}\left[1+\frac{7}{10}\frac{m_H^2}{m_i^2}\right] \\
&\quad +\frac{8}{3}s\frac{A_{ij}^2}{m_i^2}\left[1+\frac{15m_H^2-4s}{60m_i^2}-\frac{\delta}{2m_i^2}\right]+\mathcal{O}\left(\frac{s^2}{m_i^4},\frac{\delta^2}{m_i^4}\right), \\
F_2(s,t,u,m_i^2,\delta) &= \frac{Y_{ii}^2+Y_{jj}^2+2Y_{ij}^2}{m_i^2}F_2(s,t,u,m_i^2)+s\frac{Y_{jj}^2+Y_{ij}^2}{m_i^2}\frac{\delta}{m_i^2}\left(\frac{22}{45}\frac{p_T^2}{m_i^2}\right) \\
&\quad -\frac{2}{3}s\frac{A_{ij}^2}{m_i^2}\frac{p_T^2}{m_i^2}+\mathcal{O}\left(\frac{s^2}{m_i^4},\frac{\delta^2}{m_i^4}\right).
\end{aligned}
\tag{18}
$$

Following [70], we consider the infinite quark mass limit of these results and recast them into a convenient form for the calculation of the amplitudes for single and double Higgs production in models with extended quark sectors with respect to the Standard Model amplitudes. In the infinite mass approximation, the leading order amplitudes can be written as (Eqs. 16, 17)

$$
A_{gg\to H} \propto \mathrm{Tr}\left(y\mathcal{M}^{-1}\right) \qquad , \qquad A_{gg\to HH}^{box} \propto \mathrm{Tr}\left(y\mathcal{M}^{-1}y\mathcal{M}^{-1}\right),
\tag{19}
$$

12

where the omitted proportionality terms do not depend on the masses and Higgs couplings of the quarks. In the Standard Model, $y_{tt} = m_t$. The amplitudes only depend on the omitted proportionality factors, which therefore cancel when taking the ratio to the Standard Model result:

$$R_{gg \to H} \equiv \frac{A_{gg \to H}}{A_{gg \to H}^{SM}} = \mathrm{Tr}\left(y\mathcal{M}^{-1}\right) = \frac{\partial}{\partial v}\left(\log \det \mathcal{M}\right) , \tag{20}$$

$$R_{gg \to HH}^{box} \equiv \frac{A_{gg \to HH}^{box}}{A_{gg \to HH}^{box,SM}} = \mathrm{Tr}\left(y\mathcal{M}^{-1}y\mathcal{M}^{-1}\right) \tag{21}$$

In Eq. 20 we used the relation $y = \frac{\partial \mathcal{M}}{\partial v}$ [70]. Eq. 21 is equivalent to the result of Ref. [34].

III. EXAMPLES

A. Singlet top partner

We are interested in examining possible large effects in two Higgs production from gluon fusion in models which are consistent with precision electroweak measurements and the observed rate for single Higgs production. Topcolor models [23, 28], top condensate models [24–27], and little Higgs models [49–55] all contain a charge $\frac{2}{3}$ partner of the top quark. We consider a general case with a vector $SU(2)_L$ singlet fermion, $\mathcal{T}^2$, which is allowed to mix with the Standard Model like top quark, $\mathcal{T}^1$ [5, 68, 69, 71–73]. The fermions are,

$$\psi_L = \begin{pmatrix} \mathcal{T}_L^1 \\ \mathcal{B}_R^1 \end{pmatrix} , \quad \mathcal{T}_R^1, \mathcal{B}_R^1 ; \mathcal{T}_L^2, \mathcal{T}_R^2 . \tag{22}$$

Following the notation of [5], the mass eigenstates are t, T and $b = \mathcal{B}^1$ (where t, b are the observed top and bottom quarks), and can be found by the rotations

$$\chi_{L,R}^t \equiv \begin{pmatrix} t_{L,R} \\ T_{L,R} \end{pmatrix} \equiv U_{L,R}^t \begin{pmatrix} \mathcal{T}_{L,R}^1 \\ \mathcal{T}_{L,R}^2 \end{pmatrix} . \tag{23}$$

The chirality projectors are $P_{L,R} \equiv \frac{1 \mp \gamma_5}{2}$ and the mixing matrices U_L^t, U_R^t are unitary and parameterized as,

$$U_L^t = \begin{pmatrix} \cos\theta_L & -\sin\theta_L \\ \sin\theta_L & \cos\theta_L \end{pmatrix} , \quad U_R^t = \begin{pmatrix} \cos\theta_R & -\sin\theta_R \\ \sin\theta_R & \cos\theta_R \end{pmatrix} . \tag{24}$$

We will abbreviate $s_L = \sin\theta_L$, $c_L = \cos\theta_L$.

The fermion mass terms are

$$
\begin{aligned}
-\mathcal{L}_{M,1} &= \lambda_1 \overline{\psi}_L H \mathcal{B}_R^1 + \lambda_2 \overline{\psi}_L \tilde{H} \mathcal{T}_R^1 + \lambda_3 \overline{\psi}_L \tilde{H} \mathcal{T}_R^2 + \lambda_4 \overline{\mathcal{T}}_L^2 \mathcal{T}_R^1 + \lambda_5 \overline{\mathcal{T}}_L^2 \mathcal{T}_R^2 + \text{h.c.} \\
&= \overline{\chi}_L^t \left[U_L^t M_{(1)}^t U_R^{t\dagger} \right] \chi_R^t + \lambda_1 \frac{v}{\sqrt{2}} \overline{\mathcal{B}}_L^1 \mathcal{B}_R^1 + \text{h.c.} ,
\end{aligned}
\tag{25}
$$

where

$$
M_{(1)}^t = \begin{pmatrix} \lambda_2 \frac{v}{\sqrt{2}} & \lambda_3 \frac{v}{\sqrt{2}} \\ \lambda_4 & \lambda_5 \end{pmatrix} .
\tag{26}
$$

Without loss of generality, the $\overline{\mathcal{T}}_L^2 \mathcal{T}_R^1$ term can be rotated away through a redefinition of the right handed fields. The model therefore contains three independent parameters in the top sector, which we take to be m_t, M_T and θ_L. The consistency of the model with electroweak precision measurements and its decoupling properties have been studied in many works [5, 67, 69, 71–73]. We will not repeat this analysis here, but use the results of Ref. [5]. It is interesting to note that in the limit $\theta_L \sim 0$ (required by precision electroweak data), the mass terms for the top like quark and its partner become

$$
\begin{aligned}
\lambda_2 &\simeq \frac{\sqrt{2} m_t}{v} \left[1 + \frac{s_L^2}{2}(r-1) \right] , \\
\lambda_5 &\simeq M_T \left[1 + \frac{s_L^2}{2} \frac{1-r}{r} \right] ,
\end{aligned}
\tag{27}
$$

where $r = \frac{M_T^2}{m_t^2}$. Decoupling of the heavy quark therefore requires $s_L^2 \sim r^{-1}$, as it was shown in [5].

Since we are interested in Higgs production from the quark loops, we need the couplings to the Higgs boson,

$$
-\mathcal{L}_{H,1} = \frac{m_t}{v} c_{tt} \overline{t}_L t_R H + \frac{M_t}{v} c_{TT} \overline{T}_L T_R H + \frac{M_T}{v} c_{tT} \overline{t}_L T_R H + \frac{m_t}{v} c_{Tt} \overline{T}_L t_R H + \text{h.c.} ,
\tag{28}
$$

where

$$
c_{tt} = c_L^2 \qquad , \qquad c_{TT} = s_L^2 \qquad , \qquad c_{tT} = c_{Tt} = s_L c_L .
\tag{29}
$$

Using Eq. 29 and the low energy theorems of Eqs. 20 and 21, it is straightforward to see that the single and double Higgs production rates are the same as the Standard Model up to corrections of $\mathcal{O}\left(\frac{s}{m_t^2}, \frac{s}{M_T^2} \right)$. These corrections are further suppressed by the small mixing angles allowed by the bounds from electroweak precision data [5]. Both total and differential distributions are very close to the Standard Model (Fig. 8), and one cannot use
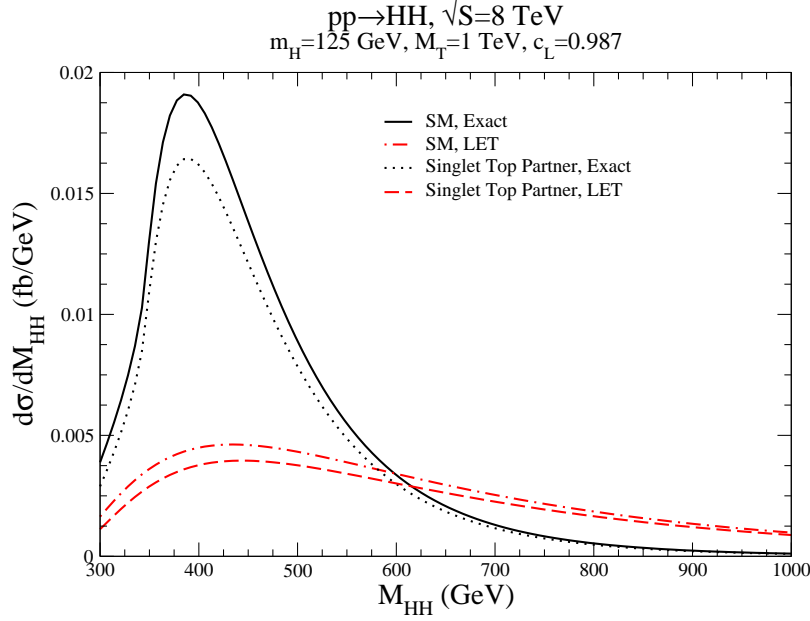
FIG. 8: Invariant mass distribution in the Standard Model and in the top-singlet partner model (with $M_T = 1$ TeV) at the $\sqrt{S} = 8$ TeV LHC.

double Higgs production to obtain information about additional vector singlet quarks. Fig. 8 uses the largest mixing angle allowed by precision electroweak data, and the reduction in the total cross section for the singlet top partner model from the exact Standard Model result is roughly 15%. This is of similar size to the reduction in the $gg \to H$ rate found in Ref. [5]. This model is an example of a case which will be extremely difficult to differentiate from the Standard Model.

B. Mirror fermions

As a second example, we consider a model which has a generation of heavy mirror fermions [71, 74–77]. There are four new quarks $\mathcal{T}^1$, $\mathcal{T}^2$ and $\mathcal{B}^1$, $\mathcal{B}^2$, with charge $\frac{2}{3}$ and $-\frac{1}{3}$, respectively. The quarks are in the $SU(2)_L$ representations,

$$\psi_L^1 = \begin{pmatrix} \mathcal{T}_L^1 \\ \mathcal{B}_L^1 \end{pmatrix}, \quad \mathcal{T}_R^1, \mathcal{B}_R^1; \qquad \psi_R^2 = \begin{pmatrix} \mathcal{T}_R^2 \\ \mathcal{B}_R^2 \end{pmatrix}, \quad \mathcal{T}_L^2, \mathcal{B}_L^2. \tag{30}$$

The first set of heavy quarks has the quantum numbers of the Standard Model quarks, while $\mathcal{T}^2$ and $\mathcal{B}^2$ have have the left- and right- handed fermion assignments reversed from those

of the Standard Model. For simplicity, we assume there is no mixing between the heavy mirror fermions and the Standard Model fermions. This assumption eliminates the need to consider limits from $Z \to b\bar{b}$ [65] and relaxes the restrictions from precision electroweak data discussed in Sec. III B 1[2].

The most general Lagrangian for the interactions of the mirror fermions with the Higgs doublet is,

$$
\begin{aligned}
-\mathcal{L} &= \lambda_A \overline{\psi}_L^1 \Phi \mathcal{B}_R^1 + \lambda_B \overline{\psi}_L^1 \tilde{\Phi} \mathcal{T}_R^1 + \lambda_C \overline{\psi}_R^2 \Phi \mathcal{B}_L^2 + \lambda_D \overline{\psi}_R^2 \tilde{\Phi} \mathcal{T}_L^2 \\
&\quad + \lambda_E \overline{\psi}_L^1 \psi_R^2 + \lambda_F \overline{\mathcal{T}}_R^1 \mathcal{T}_L^2 + \lambda_G \overline{\mathcal{B}}_R^1 \mathcal{B}_L^2 + \text{h.c.} \\
&= \overline{\chi}_L^t \left[U_L^t \mathcal{M}_U U_R^{t\dagger} \right] \chi_R^t + \overline{\chi}_L^b \left[U_L^b \mathcal{M}_D U_R^{b\dagger} \right] \chi_R^b + \text{h.c.}\,.
\end{aligned}
\tag{31}
$$

The mass eigenstates χ_P^q $(P = L, R;\, q = t, b)$ are obtained through unitary rotations

$$
U_P^q = \begin{pmatrix} \cos\theta_P^q & -\sin\theta_P^q \\ \sin\theta_P^q & \cos\theta_P^q \end{pmatrix},
\tag{32}
$$

and the mass matrices are

$$
\mathcal{M}_U = \begin{pmatrix} \lambda_B \frac{v}{\sqrt{2}} & \lambda_E \\ \lambda_F & \lambda_D \frac{v}{\sqrt{2}} \end{pmatrix}, \qquad \mathcal{M}_D = \begin{pmatrix} \lambda_A \frac{v}{\sqrt{2}} & \lambda_E \\ \lambda_G & \lambda_C \frac{v}{\sqrt{2}} \end{pmatrix}.
\tag{33}
$$

We will denote the two top- like and the two bottom- like mass eigenstates as T_1, T_2 and B_1, B_2 respectively. The Lagrangian parameters λ_i can be expressed in terms of the physical quark masses and the mixing angles. We report these relations in Appendix A.

Since all the quarks have different quantum numbers, it is not possible to rotate away any parameter in the Lagrangian. However, the $SU(2)$ symmetry requires that

$$
\mathcal{M}_{U,12} = \mathcal{M}_{D,12}\,,
\tag{34}
$$

and therefore

$$
M_{T_2} \cos\theta_R^t \sin\theta_L^t - M_{T_1} \cos\theta_L^t \sin\theta_R^t = M_{B_2} \cos\theta_R^b \sin\theta_L^b - M_{B_1} \cos\theta_L^b \sin\theta_R^b\,.
\tag{35}
$$

This relation can be written as

$$
\left[M_{T_2} + M_{T_1} \right] \sin\theta_-^t + \left[M_{T_2} - M_{T_1} \right] \sin\theta_+^t = \left[M_{B_2} + M_{B_1} \right] \sin\theta_-^b + \left[M_{B_2} - M_{B_1} \right] \sin\theta_+^b\,,
\tag{36}
$$

---

[2] We will not explore UV completions of this model that can mediate the decay of the mirror fermions through higher-dimensional operators and prevent the new quarks from becoming stable.

where $\theta_{\pm}^{t(b)} = \theta_L^{t(b)} \pm \theta_R^{t(b)}$.

The couplings of the fermion mass eigenstates to the Higgs boson are

$$-\mathcal{L}_M^H = \frac{c_{T_1T_1}}{2v}\overline{T}_{1L}T_{1R}\,H + \frac{c_{T_2T_2}}{2v}\overline{T}_{2L}T_{2R}\,H + \frac{c_{T_1T_2}}{2v}\overline{T}_{1L}T_{2R}\,H + \frac{c_{T_2T_1}}{2v}\overline{T}_{2L}T_{1R}\,H +$$
$$\frac{c_{B_1B_1}}{2v}\overline{B}_{1L}B_{1R}\,H + \frac{c_{B_2B_2}}{2v}\overline{B}_{2L}B_{2R}\,H + \frac{c_{B_1B_2}}{2v}\overline{B}_{1L}B_{2R}\,H + \frac{c_{B_2B_1}}{2v}\overline{B}_{2L}B_{1R}\,H + \text{h.c.}\,,$$
$$(37)$$

where

$$\begin{aligned}
c_{T_1T_1} &= M_{T_1}\left[1 + \cos\left(2\theta_L^t\right)\cos\left(2\theta_R^t\right)\right] + M_{T_2}\sin\left(2\theta_L^t\right)\sin\left(2\theta_R^t\right) \\
&= 2M_{T_1}\left[\cos^2\theta_-^t - \frac{M_{T_1} - M_{T_2}}{2M_{T_1}}\left(\sin^2\theta_+^t - \sin^2\theta_-^t\right)\right]\,, \\
c_{T_1T_2} &= M_{T_1}\cos\left(2\theta_L^t\right)\sin\left(2\theta_R^t\right) - M_{T_2}\cos\left(2\theta_R^t\right)\sin\left(2\theta_L^t\right) \\
&= \frac{M_{T_1} - M_{T_2}}{2}\sin(2\theta_+^t) - \frac{M_{T_2} + M_{T_1}}{2}\sin(2\theta_-^t)\,, \\
(c_{T_2T_2}, c_{T_2T_1}) &= (c_{T_1T_1}, c_{T_1T_2}) \text{ with } M_{T_1} \leftrightarrow M_{T_2}, \theta_\pm^t \to -\theta_\pm^t\,.
\end{aligned}$$
$$(38)$$

Similar expressions hold in the bottom sector.

The couplings to the electroweak gauge bosons that are needed for the computation of the Peskin–Takeuchi parameters (Sec. III B 1) are reported in the Appendix.

1. Higgs production using low energy theorems in the mirror model

For single Higgs production through top quark and mirror fermion loops, the low energy theorem of Eq. 20 yields

$$A_{gg \to H} = A_{gg \to H}^{SM}\left(1 + \frac{c_{T_1T_1}}{2M_{T_1}} + \frac{c_{T_2T_2}}{2M_{T_2}} + \frac{c_{B_1B_1}}{2M_{B_1}} + \frac{c_{B_2B_2}}{2M_{B_2}}\right) \equiv A_{gg \to H}^{SM}\left(1 + \Delta\right)\,, \quad (39)$$

where we introduce the fractional difference Δ of the single Higgs amplitude from that of the Standard Model.

Both for simplicity and because one expects large corrections to the oblique parameters for a large mass splitting within each chiral doublet, we assume $M_{T_1} = M_{B_1} = M$ and $M_{T_2} = M_{B_2} = M(1 + \delta)$. In this limit,

$$A_{gg \to H} = A_{gg \to H}^{SM}\left\{1 + 4 - \frac{1}{1+\delta}\left[(2 + \delta)\sin\theta_-^t - \delta\sin\theta_+^t\right]\left[(2 + \delta)\sin\theta_-^b + \delta\sin\theta_+^b\right]\right\}\,,$$
$$(40)$$

17

where we impose (see Eq. 36)

$$(2 + \delta) \sin \theta_-^t + \delta \sin \theta_+^t = (2 + \delta) \sin \theta_-^b + \delta \sin \theta_+^b \,. \tag{41}$$

Given the recent observations at the LHC, we are interested in the case when $A_{gg \to H} \sim A_{gg \to H}^{SM}$. One simple way to recover this limit is to have

$$\theta_-^t \sim \frac{\pi}{2}, \quad \theta_-^b \sim \frac{\pi}{2}, \tag{42}$$

which for single production gives[3]

$$A_{gg \to H} \sim A_{gg \to H}^{SM} \left\{ 1 - \frac{\delta^2}{1 + \delta} \cos^2 \theta_+^b \right\} = A_{gg \to H}^{SM} \left\{ 1 - \frac{\delta^2}{1 + \delta} \sin^2 (2\theta_R^b) \right\} \,. \tag{43}$$

To get the Standard Model result for $gg \to H$ further requires either $\delta \sim 0$ or $\theta_R^b \sim \theta_R^t \sim 0$, where the constraint on the right-handed mixing angle in the top sector arises from Eq. 41.

The result of Eq. 43 can be understood by inspecting the Yukawa couplings in the limit $\theta_-^{t,b} = \frac{\pi}{2}$:

$$c_{T_1 T_1} = -c_{T_2 T_2} = -M\delta \cos^2(\theta_+^t) = -M\delta \sin^2(2\theta_R^t) \,,$$
$$c_{T_1 T_2} = c_{T_2 T_1} = -\frac{M\delta}{2} \sin(2\theta_+^t) = \frac{M\delta}{2} \sin(4\theta_R^t) \,. \tag{44}$$

Similar relations hold for the charge $-\frac{1}{3}$ sector. Hence, for $\delta \sim 0$ or $\theta_R^{t,b} \sim 0$ the diagonal Yukawa couplings go to zero and only the top quark, with its Standard Model Yukawa coupling, contributes to single Higgs production. The off-diagonal couplings of the mirror fermions to the Higgs boson are slightly less suppressed, and could induce deviations in the double Higgs rate from that of the Standard Model.

From the low energy theorem of Eq. 21, the box contributions to $gg \to HH$ production (including top quark loops) can be estimated,

$$F_1^{box} \equiv F_1^{box,SM} (1 + \Delta_{box}) \,;$$
$$\Delta_{box} = \frac{c_{T_1 T_1}^2}{4M_{T_1}^2} + \frac{c_{T_2 T_2}^2}{4M_{T_2}^2} + \frac{c_{B_1 B_1}^2}{4M_{B_1}^2} + \frac{c_{B_2 B_2}^2}{4M_{B_2}^2} + \frac{c_{T_1 T_2} c_{T_2 T_1}}{2M_{T_1} M_{T_2}} + \frac{c_{B_1 B_2} c_{B_2 B_1}}{2M_{B_1} M_{B_2}}$$
$$= 4 + \frac{3}{2} \frac{\alpha_1^2 - \alpha_2^2 + \alpha_3^2 - \alpha_4^2}{1 + \delta} + \frac{1}{4} \frac{(\alpha_1^2 - \alpha_2^2)^2 + (\alpha_3^2 - \alpha_4^2)^2}{(\delta + 1)^2} \,, \tag{45}$$

---

[3] This relation holds for small δ. For $\delta = 0$, Eq. 36 requires $\sin \theta_-^t = \sin \theta_-^b$, and $A_{gg \to H} = A_{gg \to H}^{SM} (1 + 4 \cos^2 \theta_-^b)$. This result can be easily understood from the Yukawa couplings, $c_{T_1 T_1} = c_{T_2 T_2} = M \cos^2 \theta_-^b$ and $c_{T_2 T_1} = -c_{T_1 T_2} = \frac{M}{2} \sin(2\theta_-^b)$. Also in this case, the $gg \to H$ rate is identical to the Standard Model rate for $\theta_-^b = \frac{\pi}{2}$.

where we defined

$$\alpha_1 = \delta \sin\theta_+^b + (2+\delta)(\sin\theta_-^b - \sin\theta_-^t) \, ,$$

$$\alpha_2 = (2+\delta)\sin\theta_-^t \quad , \qquad \alpha_3 = \delta\sin\theta_+^b \quad , \qquad \alpha_4 = (2+\delta)\sin\theta_-^b \, . \qquad (46)$$

For $\theta_-^{t,b} \sim \frac{\pi}{2}$, Eq. 45 yields[4]

$$\Delta_{box} = \frac{\delta^2}{1+\delta}\cos^2\theta_+^b + \frac{\delta^4}{2(1+\delta)^2}\cos^4\theta_+^b \, . \qquad (47)$$

Note that F_2^{box} does not contribute in the infinite fermion mass limit. The terms proportional to $\cos^2(\theta_+^b)$ come from the contributions of the off-diagonal fermion-Higgs couplings. For this simple choice of parameters, the same term governs the deviations from the Standard Model both in single and double Higgs production.

We are interested in determining how large a deviation from the Standard Model $gg \to HH$ rate is possible with a minimal deviation in the $gg \to H$ rate. With the assumption of no mass splitting within the mirror doublets, there are five independent parameters: the mass scale M, which drops out in the heavy mass limit for the Higgs production rates, the mass splitting between families, δ, and three angles. Using Eq. 40, we replace one of the angles with the fractional deviation Δ of the $gg \to H$ amplitude from that of the Standard Model,

$$\sin\theta_-^b = \frac{1}{2+\delta}\left\{\frac{(4-\Delta)(1+\delta)}{(2+\delta)\sin\theta_-^t - \delta\sin\theta_+^b} - \delta\sin\theta_+^b\right\} \, . \qquad (48)$$

We require this deviation to be within 10% and the mass splitting δ between the two mirror families not to be too large ($0 < \delta < 1$), since we expect electroweak observables to put severe bounds on δ. Under these constraints, we perform a scan over $\delta, \Delta, \theta_-^t$ and θ_+^b. The values of these parameters for which Eqs. 41 and 48 yield real solutions for θ_+^t, θ_-^b are represented by the blue dots in Fig. 9. The red diamonds represent regions where the difference Δ_{box} in the double Higgs amplitude from the box topology is larger than 15%.

In the following, we fix $\theta_-^t = \frac{\pi}{2}$ in order to focus on a region with large Δ_{box}, and analyse how double Higgs production depends on θ_+^b and δ for a Standard Model $gg \to H$ amplitude, $\Delta = 0$, and for $\pm 10\%$ deviations from it, $\Delta = \pm 0.1$. This analysis is shown in Fig. 10 for a heavy mass scale $M = 800$ GeV. To qualitatively understand the features of these plots, one

---

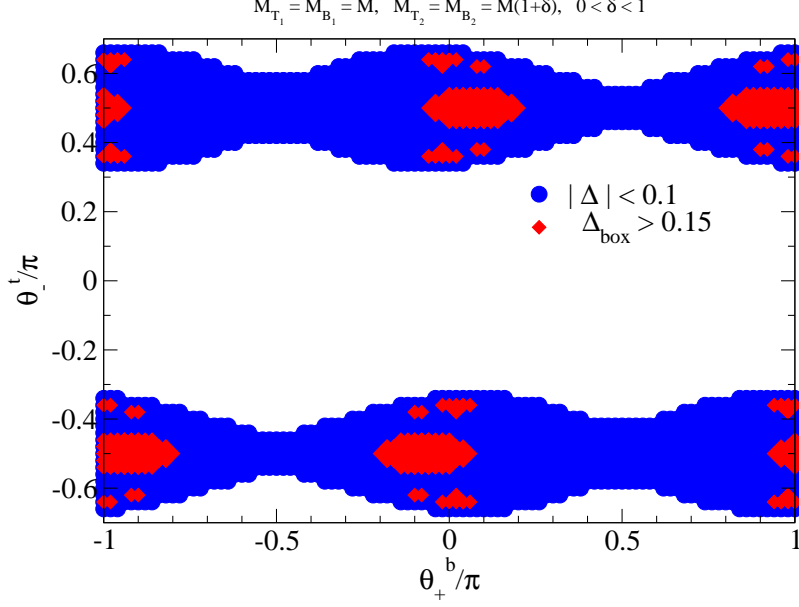[4] In the exact $\delta = 0$ limit the result reads $F_1^{box} = F_1^{box,SM}\left[1 - 4\cos^2\theta_-^b + 8\cos^4\theta_-^b\right]$.

$$M_{T_1} = M_{B_1} = M, \quad M_{T_2} = M_{B_2} = M(1+\delta), \quad 0 < \delta < 1$$

- $\bullet$ $|\Delta| < 0.1$
- $\blacklozenge$ $\Delta_{box} > 0.15$

FIG. 9: Allowed regions in the θ^t_-, θ^b_+ parameter space where deviations, Δ, from the Standard Model $gg \to H$ amplitude are below 10% and the mirror fermion masses satisfy $0 < \delta < 1$. The other two angles are fixed through Eqs. 41 and 48. The red diamonds denote regions where the $gg \to HH$ amplitude from the box topology deviates from the Standard Model by more than 15%.

can consider the limit of small deviations from the Standard Model single Higgs amplitude and small family splitting δ,

$$\Delta_{box} = \delta^4 \cos^4 \theta^b_+ \left[\frac{1}{2} - \delta(1 - \sin \theta^b_+) \right] + \Delta \left[-1 + \delta^2 \cos^2 \theta^b_+ + \mathcal{O}(\delta^3) \right] + \mathcal{O}(\Delta^2, \delta^6) . \quad (49)$$

For almost degenerate mirror fermions ($\delta \sim 0$) and small deviations in single Higgs production from the Standard Model case, (which occurs when $\theta^b_+ = \pm\frac{\pi}{2}$), the dominant term is $\Delta_{box} \sim -\Delta$. When single Higgs production is suppressed, double Higgs production is always enhanced, while for a slightly enhanced Higgs single production rate, double production can also be suppressed. For $\Delta = 0$ and small δ, double Higgs production is also enhanced. In all cases, the minimal deviations from Standard Model double Higgs production occurs exactly at $\theta^b_+ = \pm\frac{\pi}{2}$, while the maximum deviation is at

$$\theta^b_+ = \arccos \left(2\frac{\sqrt{1+\delta}}{2+\delta} \right) + \frac{\sqrt{1+\delta}}{2\delta} \Delta + \mathcal{O}(\Delta^2) . \quad (50)$$

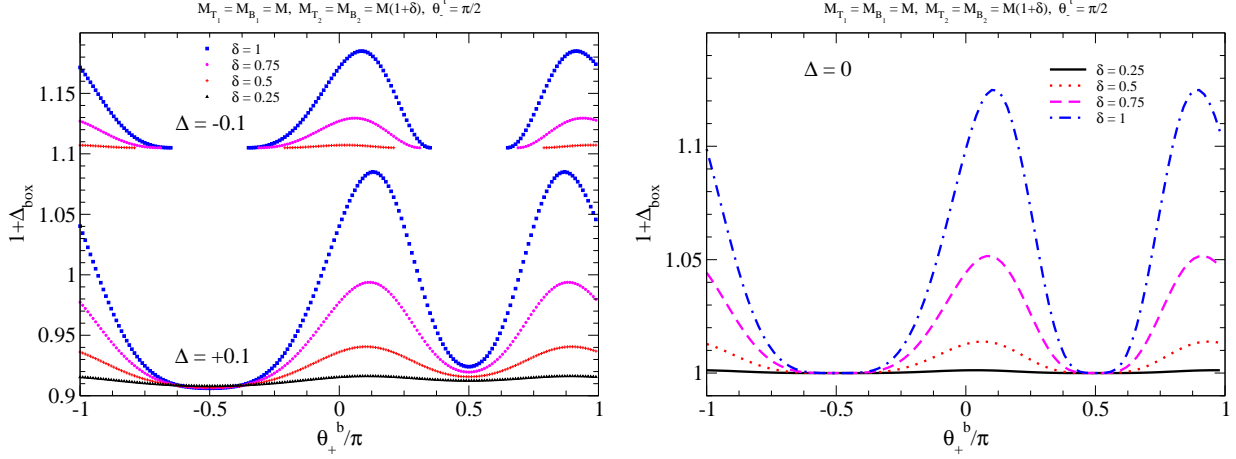Finally, we note that the results of this section can be written in terms of an effective

20

FIG. 10: Deviations from the Standard Model box amplitude, F_1^{box}, as a function of θ_+^b for $\theta_-^t = \frac{\pi}{2}$, $M = 800$ GeV and four different values of the fractional mass difference δ of the two mirror families, for a 10% deviation in the single Higgs production amplitude (left plot) and for the same $gg \to H$ amplitude as in the Standard Model (right plot). The blank regions on the curves are not allowed for θ_+^t, θ_-^b to be real.

Lagrangian, which for $\delta = 0$ is

$$\mathcal{L}_{eff} = \frac{\alpha_s}{12\pi} G_{\mu\nu}^a G^{a,\mu\nu} \left[(1 + 4\cos^2\theta_-^b)\frac{H}{v} - (1 - 4\cos^2\theta_-^b + 8\cos^4\theta_-^b)\frac{H^2}{2v^2} \right] . \tag{51}$$

2. Bounds from electroweak precision data

The new mirror quarks carry electroweak charges, and therefore contribute to the self - energies of the electroweak gauge bosons [72, 74, 78]. A convenient way to parametrize these effects is through the Peskin–Takeuchi parameters [79, 80],

$$\alpha\Delta S_F = \frac{4s_W^2 c_W^2}{M_Z^2} \left\{ \Pi_{ZZ}(M_Z^2) - \Pi_{ZZ}(0) - \Pi_{\gamma\gamma}(M_Z^2) - \frac{c_W^2 - s_W^2}{c_W s_W}\Pi_{\gamma Z}(M_Z^2) \right\} ,$$

$$\alpha\Delta T_F = \frac{\Pi_{WW}(0)}{M_W^2} - \frac{\Pi_{ZZ}(0)}{M_Z^2} ,$$

$$\alpha\Delta U_F = 4s_W^2 \left\{ \frac{\Pi_{WW}(M_W^2) - \Pi_{WW}(0)}{M_W^2} - c_W^2 \left(\frac{\Pi_{ZZ}(M_Z^2) - \Pi_{ZZ}(0)}{M_Z^2} \right) \right.$$
$$\left. -2s_W c_W \frac{\Pi_{\gamma Z}(M_Z^2)}{M_Z^2} - s_W^2 \frac{\Pi_{\gamma\gamma}(M_Z^2)}{M_Z^2} \right\} , \tag{52}$$

where $\Pi_{XY}(p^2)$ denotes the transverse part of the vacuum polarization amplitude evaluated at momentum p^2 and $c_W^2 = \frac{M_W^2}{M_Z^2} = 1 - s_W^2$. The couplings of the mirror fermions to the

electroweak gauge bosons are reported in the Appendix.

We use the fit to the electroweak precision data given in Ref. [81],

$$S = 0.03 \pm 0.10 \quad , \qquad T = 0.05 \pm 0.12 \quad , \qquad U = 0.03 \pm 0.10 \,, \tag{53}$$

with correlation coefficients

$$\rho_{ij} = \begin{pmatrix} 1.0 & 0.89 & -0.54 \\ 0.89 & 1.0 & -0.83 \\ -0.549 & -0.83 & 1.0 \end{pmatrix} \,.$$

The reference Higgs and top-quark masses are $m_{H,\text{ref}} = 126$ GeV and $m_{t,\text{ref}} = 173$ GeV. We use $m_H = 125$ GeV and so we need to account also for the Higgs contributions to the electroweak parameters. Up to terms of $\mathcal{O}(M_Z^2/m_H^2)$, they read

$$\Delta S_H = \frac{1}{12\pi} \log\left(\frac{m_H^2}{m_{H,\text{ref}}^2}\right) \quad , \qquad \Delta T_H = -\frac{3}{16\pi c_W^2} \log\left(\frac{m_H^2}{m_{H,\text{ref}}^2}\right) \quad , \qquad \Delta U_H = 0 \,. \tag{54}$$

The $\Delta\chi^2$ is defined as

$$\Delta\chi^2 = \sum_{i,j} (X_i - \hat{X}_i)(\sigma^2)_{ij}^{-1}(X_j - \hat{X}_j) \,, \tag{55}$$

where $\hat{X}_i$ are the central values of the electroweak parameters from the fit in Eq. 53, X_i are the contributions to these parameters from the new mirror fermions and from the Higgs loops, and $\sigma_{ij}^2 \equiv \sigma_i \rho_{ij} \sigma_j$, with σ_i being the errors given in Eq. 53.

We consider the case of no mass splitting within the doublets, while the fractional mass difference between the two heavy families is parametrized by δ, and focus on the regions of parameter space where we expect the largest deviations with respect to the Standard Model $gg \to HH$ amplitude, while the single Higgs rate remains very close to the Standard Model value. Following the discussion in the previous section, we therefore fix $\theta_-^t = \frac{\pi}{2}$, $\Delta = \{-0.1; 0; 0.1\}$ and choose $M = 800$ GeV. In Fig. 11 we show the 95% allowed regions in the $\{\sin\theta_+^b, \delta\}$ parameter space for the three values of Δ (red bands), along with the regions where the box enhancement is larger than 15% (blue diamonds). The experimental bounds typically require δ to be small. In this limit, the electroweak parameters assume simple expressions,

$$\begin{aligned}
\Delta S_F &= \frac{N_C}{30\pi}\Delta\left[\frac{25}{6} + 4\delta\sin\theta_+^b - \Delta\left(1 + \delta\sin\theta_+^b\right) + \mathcal{O}(\delta^2)\right] \,, \\
\Delta T_F &= \frac{N_C}{96\pi s_W^2}\frac{M^2}{M_W^2}\Delta^2\left[2 + \delta\left(\sin\theta_+^b + 2\right) + \mathcal{O}(\delta^2)\right] \,, \\
\Delta U_F &= \frac{N_C}{60\pi}\Delta^2\left[2 + \delta\sin\theta_+^b + \mathcal{O}(\delta^2)\right] \,,
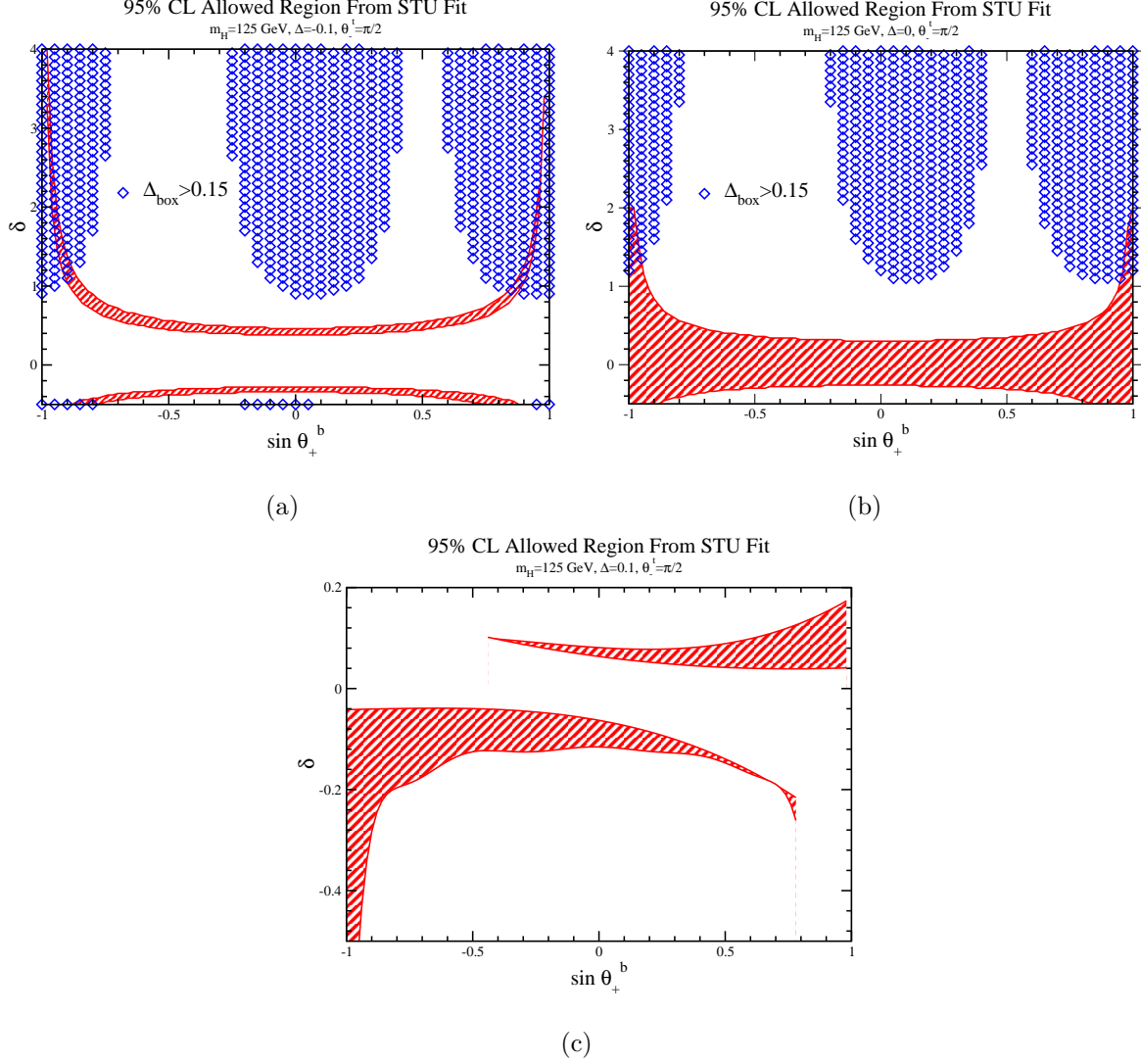\end{aligned} \tag{56}$$

22

FIG. 11: Red bands: 95% confidence level allowed regions from the fit to electroweak data for single Higgs amplitudes which are suppressed (a)/enhanced (c) by 10% with respect to the Standard Model amplitude, or equal to the Standard Model amplitude (b), for $\theta^t_- = \frac{\pi}{2}$ and $M = 800$ GeV. Blue diamonds: parameter space regions which allow an enhancement of 15% or more to the double Higgs rate from the box topology. Such a large enhancement is not allowed by electroweak precision bounds in the case of $\Delta = 0.1$ (c).

where $N_C = 3$. For $\delta \to 0$, $\theta^b_- \to \theta^t_- = \frac{\pi}{2}$ and $\Delta \to 0$ (Eq. 43). However, a large increase in the double Higgs rate from the box topology can be obtained only for large values of δ. In particular, for $\Delta = 0.1$ the electroweak precision observables do not allow the mass splitting to be large enough to obtain a significant enhancement, consistently with the results from Fig. 10.
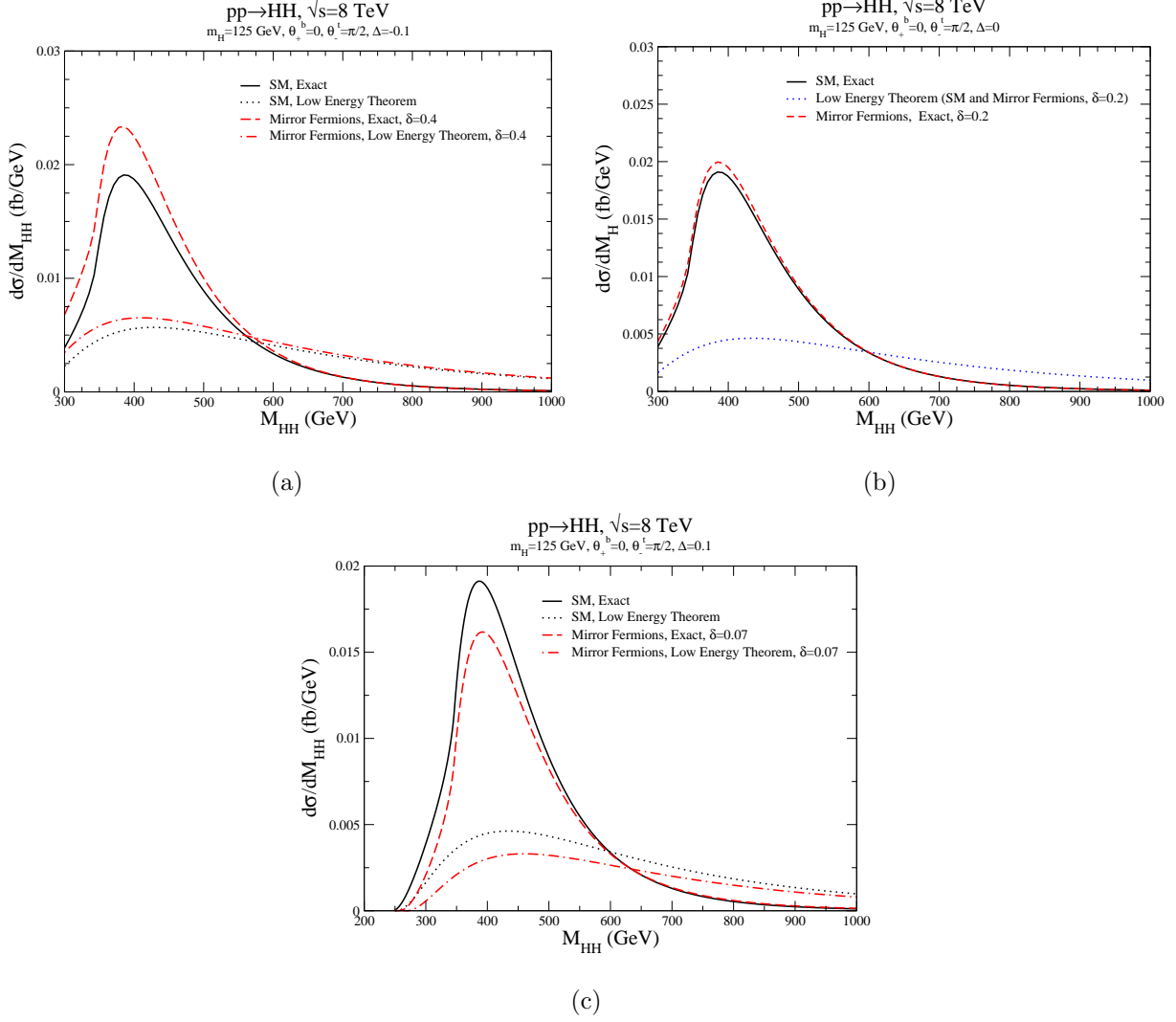
FIG. 12: Differential double Higgs production cross section in the Standard Model and in the mirror fermion model for $\theta_-^t = \frac{\pi}{2}$, $M = 800$ GeV. The single Higgs production amplitude with respect to the Standard Model is suppressed by 10% (a), equal (b) or enhanced by 10% (c). We use CT10NLO PDFs and $\mu = M_{HH} = \sqrt{s}$. The curves labelled Low Energy Theorem use the infinite mass approximation to the rate.

3. *Phenomenology of the Mirror Fermion Model and $H \to \gamma\gamma$*

Once the parameters of the model are constrained to reproduce the Standard Model single Higgs amplitude to within $\pm 10\%$ and to be allowed by a fit to the precision electroweak data, there is very little freedom left to adjust parameters. The differential cross section for $gg \to HH$ is shown for allowed parameters in Fig. 12 and it is clear that this class of

24

models does not allow for a large enhancement of the HH production rate. The exact cross sections include both Standard Model t and b contributions, while the low energy theorem curves include the infinite mass limit of the heavy quark contribution. The largest allowed enhancement is found for $\Delta = -0.1$ and in this case, the total cross section, $pp \to HH$ is enhanced by $\sim 17\%$ over the Standard Model rate.

The mirror fermions also contribute to the rate for $H \to \gamma\gamma$[5]. We again consider each mirror family to be degenerate between the charge $\frac{2}{3}$ and charge $-\frac{1}{3}$ quarks, and the two families to be split by a mass difference $M\delta$. In the limit $m_H << m_t, M_W, M$ [87],

$$\sqrt{\frac{\Gamma(H \to \gamma\gamma)}{\Gamma(H \to \gamma\gamma)_{SM}}} = 1 - \frac{16}{47}\left[\frac{c_{T_1 T_1}}{2 M_{T_1}} + \frac{c_{T_2 T_2}}{2 M_{T_2}} + \frac{1}{4}\left(\frac{c_{B_1 B_1}}{2 M_{B_1}} + \frac{c_{B_1 B_1}}{2 M_{B_2}}\right)\right]$$
$$= 1 - \frac{8}{47}\left[5 + \sin\theta_-^b \left(3\sin\theta_-^b - 8\sin\theta_-^t\right)\right]$$
$$- \frac{32}{47}\delta\sin\theta_+^b \left(\sin\theta_-^b - \sin\theta_-^t\right) + \mathcal{O}(\delta^2) , \tag{57}$$

where we impose only the angle relation from Eq. 41 and expand for small δ. In the limit $\delta = 0$ (and therefore $\theta_-^b = \theta_-^t$ from Eq. 41), the branching ratio into photons cannot be larger than in the Standard Model.

We relate the deviations in the photon decay branching ratio to the deviation Δ from the Standard Model single Higgs production rate[6],

$$\sqrt{\frac{\Gamma(H \to \gamma\gamma)}{\Gamma(H \to \gamma\gamma)_{SM}}} = 1 - \frac{24}{47}\left[\frac{4(\delta+1)}{((\delta+2)\sin\theta_-^t - \delta\sin\theta_+^b)^2} - \frac{(\delta+2)\sin\theta_-^t + \delta\sin\theta_+^b}{(\delta+2)\sin\theta_-^t - \delta\sin\theta_+^b}\right]$$
$$- \frac{4}{47}\Delta\left[1 + \frac{3(\delta+2)\sin\theta_-^t}{(\delta+2)\sin\theta_-^t - \delta\sin\theta_+^b} - \frac{12(\delta+1)}{((\delta+2)\sin\theta_-^t - \delta\sin\theta_+^b)^2}\right]$$
$$- \frac{6}{47}\Delta^2\frac{\delta+1}{((\delta+2)\sin\theta_-^t - \delta\sin\theta_+^b)^2} . \tag{58}$$

Imposing only the bounds from electroweak precision observables, and performing a general scan over the input parameters $\delta, \theta_+^b, \theta_-^b, \theta_+^t$ (fixing θ_-^t through Eq. 41, $M = 800$ GeV and δ in the range $\{-0.5; 2\}$), we find that the Higgs branching ratio into photons can have large differences from the Standard Model predictions, with suppressions as large as 90% and enhancements up to 10%. Requiring also the single Higgs production rate to be

---

[5] We consider only the contributions of heavy mirror quarks. Heavy leptons can also affect the $H \to \gamma\gamma$ rate [82–86].
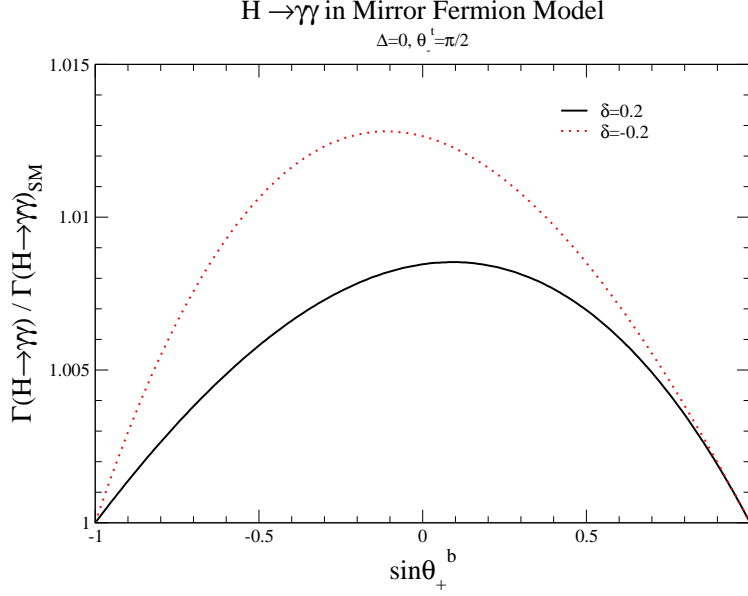
[6] This result holds for arbitrary values of the parameters.

FIG. 13: Ratio of $\Gamma(H \to \gamma\gamma)$ to the Standard Model Higgs branching ratio into photons for the points of Fig. 11(b), where $\Delta = 0$ and $\theta^t_- = \frac{\pi}{2}$. We fix $\delta = \pm 0.2$, which is allowed from the electroweak fit for all the values of θ^b_+. Larger deviations from the Standard Model $H \to \gamma\gamma$ branching ratios arise outside this range of δ, in the regions where $|\sin\theta^b_+|$ is close to 1.

close to the Standard Model value puts severe constraints on these deviations. For a single Higgs production amplitude equal to the Standard Model prediction, the maximum deviation in the Higgs branching ratio into photons is $\pm 5\%$. For the regions of parameter space of Fig. 11(a), where $\theta^t_- = \frac{\pi}{2}$ and a -10% deviation from the Standard Model prediction for the $gg \to H$ rate is allowed, only small enhancements (up to $+10\%$) of the $H \to \gamma\gamma$ rate are allowed. For a $+10\%$ enhancement in the single Higgs rate over the Standard Model prediction (Fig. 11(c)), the branching ratio into photons deviates from the Standard Model prediction by at most by a few percent. We show how these deviations depend on the free input parameters $\delta, \sin\theta^b_+$ in Fig. 13, where we focus on $\Delta = 0$ and pick two values of δ which are allowed by the electroweak fit over all the range of θ^b_+ (with $\theta^t_- = \frac{\pi}{2}$). The clear conclusion is that the restrictions from precision electroweak data, combined with a single Higgs production rate close to the Standard Model prediction, do not allow for significant deviations in the $H \to \gamma\gamma$ rate in this class of models.

IV. CONNECTION TO GLUON-HIGGS DIMENSION SIX OPERATORS

An interesting idea [36] is to combine single and double Higgs production to gain insights on the mechanism giving mass to the particles that contribute to these loop-mediated processes. Including contributions up to dimension-6 operators, the effective Lagrangian responsible for the Higgs-gluon interactions can be written as

$$\mathcal{L} = c_1 \mathcal{O}_1 + c_2 \mathcal{O}_2 \ . \tag{59}$$

Particles whose mass arises entirely from renormalizable Higgs couplings induce an operator

$$\mathcal{O}_2 = \frac{\alpha_s}{24\pi} G^a_{\mu\nu} G^{a,\mu\nu} \log\left(\frac{\Phi^\dagger \Phi}{v^2}\right) \simeq \frac{\alpha_s}{12\pi} G^a_{\mu\nu} G^{a,\mu\nu} \left(\frac{H}{v} - \frac{H^2}{2v^2}\right) \ . \tag{60}$$

If the particle receives contributions to its mass from other sources as well, an additional operator

$$\mathcal{O}_1 = \frac{\alpha_s}{12\pi} G^a_{\mu\nu} G^{a,\mu\nu} \left(\frac{\Phi^\dagger \Phi}{v^2}\right) \simeq \frac{\alpha_s}{12\pi} G^a_{\mu\nu} G^{a,\mu\nu} \left(\frac{H}{v} + \frac{H^2}{2v^2}\right) \tag{61}$$

arises. In the Standard Model $c_1^{SM} = 0$, $c_2^{SM} = 1$. The two operators contribute differently to Higgs single and pair production and the different rates in these channels constrain the coefficients c_1 and c_2. Following [36], one can derive these two coefficients in a background field approach. The Higgs field is treated as a background field, and the masses of the heavy particles become thresholds in the running of α_s. Matching the low- and high-energy theories [47, 88],

$$\frac{1}{g_{eff}^2(\mu)} = \frac{1}{g_s^2(\mu)} - \frac{\delta b_f}{8\pi^2} \log \det \frac{\mathcal{M}(H)}{\mu} \ , \tag{62}$$

where $\mathcal{M}(H)$ is the Higgs-dependent mass matrix and $\delta b_f = 2/3$ for fermions in the fundamental representation of the color group. This yields the effective Lagrangian

$$\mathcal{L}_{eff} = \frac{\alpha_s}{12\pi} G^a_{\mu\nu} G^{a,\mu\nu} \log \det \mathcal{M}(H) \ . \tag{63}$$

We write the determinant of the mass matrix as

$$\det \mathcal{M}(H) = [1 + F_i(H/v)] \times P(\lambda_i, m_i, v) \ , \tag{64}$$

where P is a polynomial of the Yukawa couplings λ_i and fermionic masses m_i and in general $F_i(H/v) = F(H/v, \lambda_i, m_i, v)$. If $F_i(H/v)$ is such that $F_i'(0) = 1 + F_i(0)$, and all the higher order derivatives vanish before electroweak symmetry breaking, then the Higgs production

27

rates via gluon fusion in the heavy quark limit are exactly as in the Standard Model[7]. This is the case in the singlet top partner model, where $F_i(H/v) = H/v$ and therefore $c_{1,2} = c_{1,2}^{SM}$.

Interestingly, one can have the same single Higgs production rate as in the Standard Model, but a different double Higgs rate, only for $F_i''(0) \neq 0$. If also the first condition, $F_i'(0) = 1 + F_i(0)$, is not met, then the single Higgs rate is not Standard Model like. In such a case, we note that for F_i independent of Yukawa couplings and fermionic masses, the Higgs rates do not depend on the details of the fermion sector [34] and deviations can arise only from changes to the Higgs potential. If F_i depends on the Yukawa couplings and fermionic masses, the Higgs rates will in general be related to these parameters. Such a situation occurs for example in the mirror fermion model. In this case

$$c_1^t = \frac{-2\beta_t}{(1-\beta_t)^2} \quad , \quad c_1^b = \frac{-2\beta_b}{(1-\beta_b)^2} \, ,$$

$$(65)$$

$$c_2^t = 1 + \frac{2}{(1-\beta_t)^2} \quad , \quad c_2^b = \frac{2}{(1-\beta_b)^2} \, .$$

We define

$$\beta_t = \frac{\lambda_E \lambda_F}{\lambda_B \lambda_D v^2/2} \quad , \qquad \beta_b = \frac{\lambda_E \lambda_G}{\lambda_A \lambda_C v^2/2} \, . \tag{66}$$

In terms of the physical parameters,

$$\beta_q = 1 - \frac{4(1+\delta)}{(2+\delta)^2 \cos^2 \theta_-^q - \delta^2 \cos^2 \theta_+^q} \, , \qquad q = t, b \, . \tag{67}$$

For $\beta_b \to 0$, c_1^b and c_2^b go to twice the Standard Model value. In this limit, the vector contributions to the fermion mass matrix vanish, and the masses come entirely from electroweak symmetry breaking. Since there are two quarks, an extra factor of two arises. In c_2^t one clearly sees the $+1$ contribution coming from the Standard Model top quark.

The coefficients governing single and double Higgs production are then

$$c_H \equiv c_1 + c_2 = 1 + 2 \left[\frac{1}{1-\beta_t} + \frac{1}{1-\beta_b} \right] \, ,$$

$$c_{HH} \equiv c_1 - c_2 = -1 - 2 \left[\frac{1+\beta_t}{(1-\beta_t)^2} + \frac{1+\beta_b}{(1-\beta_b)^2} \right] \, . \tag{68}$$

The two rates depend on the two independent parameters β_t, β_b from the top and bottom sectors. Even if we require the single Higgs rate, $gg \to H$, to be close to the Standard Model

---

[7] For the purpose of this discussion, we only need $F_i''(0) = 0$. Nonvanishing derivatives at higher orders only affect gluon fusion production of three or more Higgs bosons.
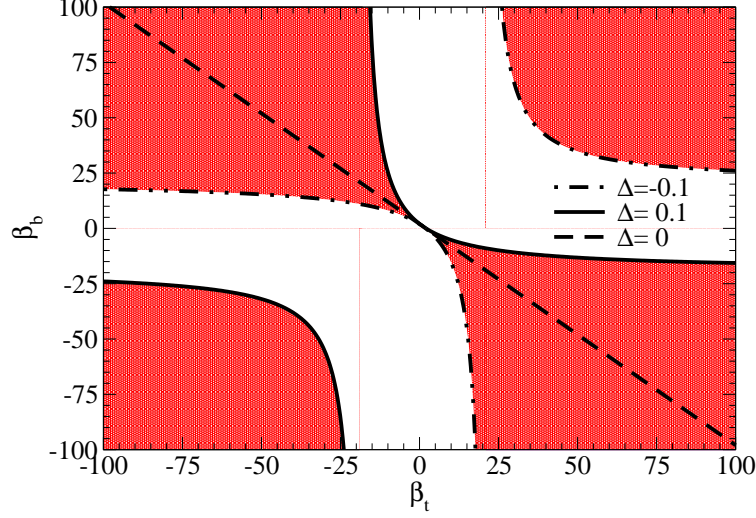
FIG. 14: The shaded red regions correspond to amplitudes for $gg \rightarrow H$ within $\pm 10\%$ of the Standard Model rate.

value,

$$c_H = c_1 + c_2 \rightarrow c_H^{SM}(1 + \Delta) = 1 + \Delta \,, \tag{69}$$

we are left with an independent parameter that can yield completely independent variations in the double Higgs rate.

In Fig. 14, we show the regions of β_b and β_t which reproduce the Standard Model Higgs amplitude to within $\Delta = \pm 10\%$. Imposing the constraint of Eq. 69 on the single Higgs rate in general constrains the double Higgs rate, $gg \rightarrow HH$,

$$c_{HH} \rightarrow 2c_1 - (1 + \Delta). \tag{70}$$

In the singlet case, $c_1 = 0$ and deviations in single and double Higgs rates must be of the same order of magnitude. In the mirror case, c_1 can deviate from zero, which removes the close relationship between single and double Higgs production.

In terms of the parameters of the mirror fermion model,

$$\begin{aligned}
c_{HH} &\rightarrow c_{HH}^{SM}\left(1 + \frac{8}{(1-\beta_t)^2} - \frac{5-\beta_t}{1-\beta_t}\Delta + \Delta^2\right) \\
&= -\left\{1 + \frac{1}{2}\left[\frac{(2+\delta)^2 \cos^2 \theta_-^t - \delta^2 \cos^2 \theta_+^t}{1+\delta}\right]^2 + \mathcal{O}(\Delta)\right\} .
\end{aligned} \tag{71}$$

The term in the curly brackets correctly reproduces $1 + \Delta_{box}$ from Eq. 49 for $\Delta = 0, \theta_-^t = \frac{\pi}{2}$. A large effect in the double Higgs rate requires large c_1, and, in turn, $\beta_t \sim 1$. This is seen
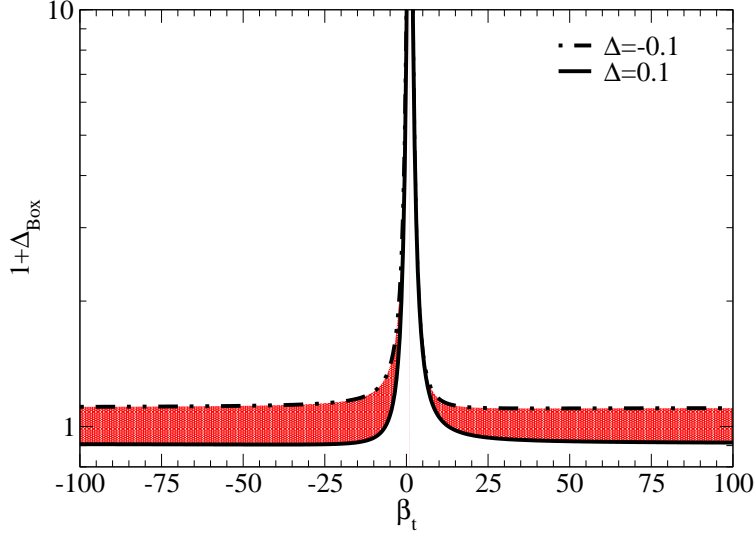
29

FIG. 15: Enhancement of the box contribution to $gg \to HH$ for a single Higgs amplitude within $\pm 10\%$ of the Standard Model prediction.

in Fig. 15, where we fix β_b to reproduce the single Higgs rate within 10% the Standard Model value. However, from Eq. 67 $\beta_t \to 1$ implies $\delta \to -1$ or $\delta \to \infty$. These are not viable solutions. The first one corresponds to massless quarks. The second one requires non-perturbative interactions with the Higgs (large λ_B, λ_D) for heavy quarks (large λ_E, λ_F), as in Eq. 66. In the mirror fermion model discussed in this paper, large deviations in the $gg \to HH$ rate do not occur.

V. CONCLUSIONS

We analysed double Higgs production from $gg \to HH$ in the Standard Model and in models with additional heavy vector or chiral quarks. In the Standard Model, we compared the approximate results in the large top mass expansion with the exact cross section, and analysed the dependence of the production rate on the choice of the renormalization/factorization scale μ and on the PDF sets. As is well known [42, 57], the low energy theorems fail to accurately reproduce both the total and differential double Higgs cross sections. The differential distributions are poorly estimated by the low energy theorems and predict a large tail at high invariant masses. The discrepancy is smallest for the scale choice $\mu = 2m_H$, yielding a $10 - 25\%$ difference from the exact calculation of the total rate. Further, the predictions of the large top mass expansion depend sensitively on the choice of PDFs. Inclusion of higher

order terms in the large mass expansion does not improve the convergence towards the exact results.

We discussed how the combination of single and double Higgs production from gluon fusion might give insight into the mechanism giving mass to quarks. The parameters of models with new heavy fermions are strongly constrained both by the observed rate for $gg \to H$ and by precision electroweak measurements. In the case of a new heavy vector singlet quark, electroweak precision observables strongly constrain its mixing with the top quark [5]. The singlet needs almost to decouple from the Standard Model particles, and therefore deviations from the Standard Model in both the single and double Higgs rates are small.

The situation is more interesting in the case of heavy mirror quarks which are not allowed to mix with the Standard Model fermions. The bounds from electroweak precision data still allow for the single Higgs production cross section to differ from the Standard Model predictions. However, after restricting the deviations in the $gg \to H$ rate from the Standard Model rate to be small, the resulting double Higgs cross section and distributions become close to those of the Standard Model. The reason for this behaviour becomes clear in terms of the two dimension six operators $\mathcal{O}_1$ and $\mathcal{O}_2$. Once we fix the single Higgs rate to be close to that of the Standard Model, large deviations in the double Higgs rate occur only if one of the mirror family becomes very heavy, with non-perturbative Higgs interactions, or very light, outside the range $m_H < 2m_q$ where the operator expansion applies. In the mirror fermion model we also investigated the effects of the additional quarks on the Higgs branching ratio to photons. After the constraints from the observed single Higgs cross section and precision electroweak measurements are taken into account, the branching ratio $H \to \gamma\gamma$ is always within 10% of the Standard Model rate.

Therefore, in the two example of models with new heavy fermions which we studied, the constraints from the observed $gg \to H$ rate, combined with precision electroweak data, do not allow large deviations of the $gg \to HH$ rate from the Standard Model prediction.

Acknowledgments

Appendix A: Electroweak parameters in the mirror fermion model

We present here some useful formulae for the mirror fermion model.

The parameters λ_i appearing in the mass Lagrangian 31 can be expressed in terms of the physical masses and mixing angles as

$$
\begin{aligned}
\lambda_2 \frac{v}{\sqrt{2}} &= m_t \, , \\
\lambda_B \frac{v}{\sqrt{2}} &= M_{T_1} \cos\theta_L^t \cos\theta_R^t + M_{T_2} \sin\theta_L^t \sin\theta_R^t \, , \\
\lambda_D \frac{v}{\sqrt{2}} &= M_{T_1} \sin\theta_L^t \sin\theta_R^t + M_{T2} \cos\theta_L^t \cos\theta_R^t \, , \\
\lambda_E &= M_{T_2} \sin\theta_L^t \cos\theta_R^t - M_{T_1} \cos\theta_L^t \sin\theta_R^t \, , \\
\lambda_F &= M_{T_2} \cos\theta_L^t \sin\theta_R^t - M_{T_1} \cos\theta_R^t \sin\theta_L^t \, .
\end{aligned}
\tag{A1}
$$

Similar relations hold for the corresponding parameters in the bottom sector, with $M_{T_i} \to M_{B_i}$ and $\theta_P^t \to \theta_P^b$.

The charged current interactions among quarks of charge Q and $(Q-1)$ are

$$
\mathcal{L}_M^{CC} = \frac{g}{\sqrt{2}} \sum_{i,j} \left\{ \bar{q}_Q^i \gamma^\mu \left[V_{ij}^L P_L + V_{ij}^R P_R \right] q_{(Q-1)}^j \right\} W_\mu^+ + \text{h.c.} \, ,
\tag{A2}
$$

with

$$
\begin{aligned}
V_{T_1 B_1}^L &= \cos\theta_L^b \cos\theta_L^t & V_{T_1 B_2}^L &= \sin\theta_L^b \cos\theta_L^t \\
V_{T_2 B_1}^L &= \cos\theta_L^b \sin\theta_L^t & V_{T_2 B_2}^L &= \sin\theta_L^b \sin\theta_L^t \\
V_{T_1 B_1}^R &= \sin\theta_R^b \sin\theta_R^t & V_{T_1 B_2}^R &= -\cos\theta_R^b \sin\theta_R^t \\
V_{T_2 B_1}^R &= -\sin\theta_R^b \cos\theta_R^t & V_{T_2 B_2}^R &= \cos\theta_R^b \cos\theta_R^t \, .
\end{aligned}
\tag{A3}
$$

We can rewrite these relations as

$$
V_{ij}^L = \left(U_L^t \right)_{i1} \left(U_L^b \right)_{j1} \, , \qquad V_{ij}^R = \left(U_R^t \right)_{i2} \left(U_R^b \right)_{j2} \, .
\tag{A4}
$$

The neutral current interactions among quarks of charge Q are

$$
\mathcal{L}_M^{NC} = \frac{g}{2c_W} \sum_{i,j} \left\{ \bar{q}_Q^i \gamma^\mu \left[X_{ij}^L P_L + X_{ij}^R P_R - 2 s_W^2 Q \delta_{ij} \right] q_Q^j \right\} Z_\mu + \text{h.c.} \, ,
\tag{A5}
$$

where

$$
\begin{aligned}
X_{T_1 T_1}^L &= \cos^2\theta_L^t & X_{T_1 T_2}^L = X_{T_2 T_1}^L &= \sin\theta_L^t \cos\theta_L^t & X_{T_2 T_2}^L &= \sin^2\theta_L^t \\
X_{T_1 T_1}^R &= \sin^2\theta_R^t & X_{T_1 T_2}^R = X_{T_2 T_1}^R &= -\sin\theta_R^t \cos\theta_R^t & X_{T_2 T_2}^R &= \cos^2\theta_R^t \, .
\end{aligned}
\tag{A6}
$$

The same relations, up to an overall minus sign, hold in the bottom sector. In more compact form we can write

$$X_{ij}^L = \pm \left(U_L^{t,b} \right)_{i1} \left(U_L^{t,b} \right)_{j1}, \qquad X_{ij}^R = \pm \left(U_R^{t,b} \right)_{i2} \left(U_R^{t,b} \right)_{j2}, \qquad (A7)$$

where the plus sign holds in the top sector and the minus in the bottom sector.

[1] Georges Aad et al. Observation of a new particle in the search for the Standard Model Higgs boson with the ATLAS detector at the LHC. *Phys.Lett.*, B716:1–29, 2012, 1207.7214.

[2] Serguei Chatrchyan et al. Observation of a new boson at a mass of 125 GeV with the CMS experiment at the LHC. *Phys.Lett.*, B716:30–61, 2012, 1207.7235.

[3] Graham D. Kribs and Adam Martin. Enhanced di-Higgs Production through Light Colored Scalars. 2012, 1207.4496.

[4] Bogdan A. Dobrescu, Graham D. Kribs, and Adam Martin. Higgs Underproduction at the LHC. *Phys.Rev.*, D85:074031, 2012, 1112.2208.

[5] S. Dawson and E. Furlan. A Higgs Conundrum with Vector Fermions. *Phys.Rev.*, D86:015021, 2012, 1205.4733.

[6] Giacomo Cacciapaglia, Aldo Deandrea, Luca Panizzi, Naveen Gaur, Daisuke Harada, et al. Heavy Vector-like Top Partners at the LHC and flavour constraints. *JHEP*, 1203:070, 2012, 1108.6329.

[7] Dean Carmi, Adam Falkowski, Eric Kuflik, and Tomer Volansky. Interpreting LHC Higgs Results from Natural New Physics Perspective. *JHEP*, 1207:136, 2012, 1202.3144.

[8] Vernon Barger, Muneyuki Ishida, and Wai-Yee Keung. Total Width of 125 GeV Higgs Boson. *Phys.Rev.Lett.*, 108:261801, 2012, 1203.3456.

[9] A. Azatov, O. Bondu, A. Falkowski, M. Felcini, S. Gascon-Shotkin, et al. Higgs boson production via vector-like top-partner decays: Diphoton or multilepton plus multijets channels at the LHC. *Phys.Rev.*, D85:115022, 2012, 1204.0455.

[10] Kunal Kumar, Roberto Vega-Morales, and Felix Yu. Effects from New Colored States and the Higgs Portal on Gluon Fusion and Higgs Decays. 2012, 1205.4244.

[11] Lei Wang and Xiao-Fang Han. The recent Higgs boson data and Higgs triplet model with vector-like quark. *Phys.Rev.*, D86:095007, 2012, 1206.1673.

[12] Nicolas Bonne and Gregory Moreau. Reproducing the Higgs boson data with vector-like quarks. *Phys.Lett.*, B717:409–419, 2012, 1206.3360.

[13] M.B. Voloshin. CP Violation in Higgs Diphoton Decay in Models with Vectorlike Heavy Fermions. 2012, 1208.4303.

[14] Enrico Bertuzzo, Pedro A.N. Machado, and Renata Zukanovich Funchal. Can New Colored Particles Illuminate the Higgs? 2012, 1209.6359.

[15] G. Moreau. Constraining extra-fermion(s) from the Higgs boson data. 2012, 1210.3977.

[16] Charalampos Anastasiou, Radja Boughezal, and Elisabetta Furlan. The NNLO gluon fusion Higgs production cross-section with many heavy quarks. *JHEP*, 1006:101, 2010, 1003.4677.

[17] Charalampos Anastasiou, Stephan Buehler, Elisabetta Furlan, Franz Herzog, and Achilleas Lazopoulos. Higgs production cross-section in a Standard Model with four generations at the LHC. *Phys.Lett.*, B702:224–227, 2011, 1103.3645.

[18] Abdelhak Djouadi and Alexander Lenz. Sealing the fate of a fourth generation of fermions. *Phys.Lett.*, B715:310–314, 2012, 1204.1252.

[19] A. Denner, S. Dittmaier, A. Muck, G. Passarino, M. Spira, et al. Higgs Production and Decay with a Fourth Standard-Model-Like Fermion Generation. *Eur.Phys.J.*, C72:1992, 2012, 1111.6395.

[20] Otto Eberhardt, Geoffrey Herbert, Heiko Lacker, Alexander Lenz, Andreas Menzel, et al. Impact of a Higgs boson at a mass of 126 GeV on the standard model with three and four fermion generations. 2012, 1209.1101.

[21] Update of the combination of higgs boson searches in pp collisions at $\sqrt(s) = 7$ tev with the atlas experiment at the lhc. Technical Report ATLAS-CONF-2011-135, CERN, Geneva, Sep 2011.

[22] The CMS collaboration. Combined results of searches for a Higgs boson in the context of the Standard Model and Beyond-Standard Models.

[23] Christopher T. Hill. Topcolor: Top quark condensation in a gauge extension of the standard model. *Phys.Lett.*, B266:419–424, 1991.

[24] Bogdan A. Dobrescu and Christopher T. Hill. Electroweak symmetry breaking via top condensation seesaw. *Phys.Rev.Lett.*, 81:2634–2637, 1998, hep-ph/9712319.

[25] R. Sekhar Chivukula, Bogdan A. Dobrescu, Howard Georgi, and Christopher T. Hill. Top quark seesaw theory of electroweak symmetry breaking. *Phys.Rev.*, D59:075003, 1999, hep-

ph/9809470.

[26] Hong-Jian He, Timothy M.P. Tait, and C.P. Yuan. New top flavor models with seesaw mechanism. *Phys.Rev.*, D62:011702, 2000, hep-ph/9911266.

[27] Hong-Jian He, Christopher T. Hill, and Timothy M.P. Tait. Top quark seesaw, vacuum structure and electroweak precision constraints. *Phys.Rev.*, D65:055006, 2002, hep-ph/0108041.

[28] Christopher T. Hill and Elizabeth H. Simmons. Strong dynamics and electroweak symmetry breaking. *Phys.Rept.*, 381:235–402, 2003, hep-ph/0203079.

[29] Kaustubh Agashe, Roberto Contino, and Alex Pomarol. The Minimal composite Higgs model. *Nucl.Phys.*, B719:165–187, 2005, hep-ph/0412089.

[30] Kaustubh Agashe, Roberto Contino, Leandro Da Rold, and Alex Pomarol. A Custodial symmetry for Zb anti-b. *Phys.Lett.*, B641:62–66, 2006, hep-ph/0605341.

[31] G.F. Giudice, C. Grojean, A. Pomarol, and R. Rattazzi. The Strongly-Interacting Light Higgs. *JHEP*, 0706:045, 2007, hep-ph/0703164.

[32] J.R. Espinosa, C. Grojean, and M. Muhlleitner. Composite Higgs Search at the LHC. *JHEP*, 1005:065, 2010, 1003.3251.

[33] R. Grober and M. Muhlleitner. Composite Higgs Boson Pair Production at the LHC. *JHEP*, 1106:020, 2011, 1012.1562.

[34] M. Gillioz, R. Grober, C. Grojean, M. Muhlleitner, and E. Salvioni. Higgs Low-Energy Theorem (and its corrections) in Composite Models. 2012, 1206.7120.

[35] Aneesh V. Manohar and Mark B. Wise. Modifications to the properties of the Higgs boson. *Phys.Lett.*, B636:107–113, 2006, hep-ph/0601212.

[36] Aaron Pierce, Jesse Thaler, and Lian-Tao Wang. Disentangling Dimension Six Operators through Di-Higgs Boson Production. *JHEP*, 0705:070, 2007, hep-ph/0609049.

[37] T. Plehn, M. Spira, and P.M. Zerwas. Pair production of neutral Higgs particles in gluon-gluon collisions. *Nucl.Phys.*, B479:46–64, 1996, hep-ph/9603205.

[38] E.W. Nigel Glover and J.J. van der Bij. HIGGS BOSON PAIR PRODUCTION VIA GLUON FUSION. *Nucl.Phys.*, B309:282, 1988.

[39] A. Djouadi, W. Kilian, M. Muhlleitner, and P.M. Zerwas. Production of neutral Higgs boson pairs at LHC. *Eur.Phys.J.*, C10:45–49, 1999, hep-ph/9904287.

[40] Matthew J. Dolan, Christoph Englert, and Michael Spannowsky. Higgs self-coupling measurements at the LHC. 2012, 1206.5001.

[41] S. Dawson, S. Dittmaier, and M. Spira. Neutral Higgs boson pair production at hadron colliders: QCD corrections. *Phys.Rev.*, D58:115012, 1998, hep-ph/9805244.

[42] T. Binoth, S. Karg, N. Kauer, and R. Ruckl. Multi-Higgs boson production in the Standard Model and beyond. *Phys.Rev.*, D74:113008, 2006, hep-ph/0608057.

[43] U. Baur, T. Plehn, and David L. Rainwater. Probing the Higgs selfcoupling at hadron colliders using rare decays. *Phys.Rev.*, D69:053004, 2004, hep-ph/0310056.

[44] Andreas Papaefstathiou, Li Lin Yang, and Jose Zurita. Higgs boson pair production at the LHC in the $b\bar{b}W^+W^-$ channel. 2012, 1209.1489.

[45] Roberto Contino, Margherita Ghezzi, Mauro Moretti, Giuliano Panico, Fulvio Piccinini, et al. Anomalous Couplings in Double Higgs Production. *JHEP*, 1208:154, 2012, 1205.5444.

[46] Roberto Contino, Christophe Grojean, Mauro Moretti, Fulvio Piccinini, and Riccardo Rattazzi. Strong Double Higgs Production at the LHC. *JHEP*, 1005:089, 2010, 1002.1011.

[47] Bernd A. Kniehl and Michael Spira. Low-energy theorems in Higgs physics. *Z.Phys.*, C69:77–88, 1995, hep-ph/9505225.

[48] Ian Low, Riccardo Rattazzi, and Alessandro Vichi. Theoretical Constraints on the Higgs Effective Couplings. *JHEP*, 1004:126, 2010, 0907.5413.

[49] N. Arkani-Hamed, A.G. Cohen, E. Katz, and A.E. Nelson. The Littlest Higgs. *JHEP*, 0207:034, 2002, hep-ph/0206021.

[50] Ian Low, Witold Skiba, and David Tucker-Smith. Little Higgses from an antisymmetric condensate. *Phys.Rev.*, D66:072001, 2002, hep-ph/0207243.

[51] Maxim Perelstein, Michael E. Peskin, and Aaron Pierce. Top quarks and electroweak symmetry breaking in little Higgs models. *Phys.Rev.*, D69:075002, 2004, hep-ph/0310039.

[52] Spencer Chang and Jay G. Wacker. Little Higgs and custodial SU(2). *Phys.Rev.*, D69:035002, 2004, hep-ph/0303001.

[53] Mu-Chun Chen and Sally Dawson. One loop radiative corrections to the rho parameter in the littlest Higgs model. *Phys.Rev.*, D70:015003, 2004, hep-ph/0311032.

[54] Jay Hubisz, Patrick Meade, Andrew Noble, and Maxim Perelstein. Electroweak precision constraints on the littlest Higgs model with T parity. *JHEP*, 0601:135, 2006, hep-ph/0506042.

[55] Tao Han, Heather E. Logan, and Lian-Tao Wang. Smoking-gun signatures of little Higgs models. *JHEP*, 0601:099, 2006, hep-ph/0506313.

[56] Claudio O. Dib, Rogerio Rosenfeld, and Alfonso Zerwekh. Double Higgs production and

quadratic divergence cancellation in little Higgs models with T parity. *JHEP*, 0605:074, 2006, hep-ph/0509179.

[57] Ulrich Baur, Tilman Plehn, and David L. Rainwater. Measuring the Higgs boson self coupling at the LHC and finite top mass matrix elements. *Phys.Rev.Lett.*, 89:151801, 2002, hep-ph/0206024.

[58] Hung-Liang Lai, Marco Guzzi, Joey Huston, Zhao Li, Pavel M. Nadolsky, et al. New parton distributions for collider physics. *Phys.Rev.*, D82:074024, 2010, 1007.2241.

[59] Robert V. Harlander and Kemal J. Ozeren. Finite top mass effects for hadronic Higgs production at next-to-next-to-leading order. *JHEP*, 0911:088, 2009, 0909.3420.

[60] Alexey Pak, Mikhail Rogal, and Matthias Steinhauser. Finite top quark mass effects in NNLO Higgs boson production at LHC. *JHEP*, 1002:025, 2010, 0911.4662.

[61] Robert V. Harlander, Hendrik Mantler, Simone Marzani, and Kemal J. Ozeren. Higgs production in gluon fusion at next-to-next-to-leading order QCD for finite top mass. *Eur.Phys.J.*, C66:359–372, 2010, 0912.2104.

[62] Alexey Pak, Mikhail Rogal, and Matthias Steinhauser. Production of scalar and pseudo-scalar Higgs bosons to next-to-next-to-leading order at hadron colliders. *JHEP*, 1109:088, 2011, 1107.3391.

[63] Robert V. Harlander, Tobias Neumann, Kemal J. Ozeren, and Marius Wiesemann. Top-mass effects in differential Higgs production through gluon fusion at order α_s^4. *JHEP*, 1208:139, 2012, 1206.0157.

[64] Nima Arkani-Hamed, Andrew G. Cohen, Thomas Gregoire, and Jay G. Wacker. Phenomenology of electroweak symmetry breaking from theory space. *JHEP*, 0208:020, 2002, hep-ph/0202089.

[65] P. Bamert, C.P. Burgess, James M. Cline, David London, and E. Nardi. R(b) and new physics: A Comprehensive analysis. *Phys.Rev.*, D54:4275–4300, 1996, hep-ph/9602438.

[66] F. del Aguila, M. Perez-Victoria, and Jose Santiago. Observable contributions of new exotic quarks to quark mixing. *JHEP*, 0009:011, 2000, hep-ph/0007316.

[67] Yasuhiro Okada and Luca Panizzi. LHC signatures of vector-like quarks. 2012, 1207.5607.

[68] Giacomo Cacciapaglia, Aldo Deandrea, Daisuke Harada, and Yasuhiro Okada. Bounds and Decays of New Heavy Vector-like Top Partners. *JHEP*, 1011:159, 2010, 1007.2933.

[69] J.A. Aguilar-Saavedra. Effects of mixing with quark singlets. *Phys.Rev.*, D67:035003, 2003,

hep-ph/0210112.

[70] Adam Falkowski. Pseudo-goldstone Higgs production via gluon fusion. *Phys.Rev.*, D77:055018, 2008, 0711.0828.

[71] L. Lavoura and Joao P. Silva. Bounds on the mixing of the down type quarks with vector - like singlet quarks. *Phys.Rev.*, D47:1117–1126, 1993.

[72] Nobuhiro Maekawa. Electroweak symmetry breaking by vector - like fermions' condensation with small S and T parameters. *Phys.Rev.*, D52:1684–1692, 1995.

[73] Marko B. Popovic and Elizabeth H. Simmons. Weak singlet fermions: Models and constraints. *Phys.Rev.*, D62:035002, 2000, hep-ph/0001302.

[74] Hong-Jian He, Nir Polonsky, and Shu-fang Su. Extra families, Higgs spectrum and oblique corrections. *Phys.Rev.*, D64:053004, 2001, hep-ph/0102144.

[75] Jens Erler and Paul Langacker. Precision Constraints on Extra Fermion Generations. *Phys.Rev.Lett.*, 105:031801, 2010, 1003.3211.

[76] Otto Eberhardt, Alexander Lenz, and Jurgen Rohrwild. Less space for a new family of fermions. *Phys.Rev.*, D82:095006, 2010, 1005.3505.

[77] Stephen P. Martin. Extra vector-like matter and the lightest Higgs scalar boson mass in low-energy supersymmetry. *Phys.Rev.*, D81:035004, 2010, 0910.2732.

[78] L. Lavoura and Joao P. Silva. The Oblique corrections from vector - like singlet and doublet quarks. *Phys.Rev.*, D47:2046–2057, 1993.

[79] Guido Altarelli and Riccardo Barbieri. Vacuum polarization effects of new physics on electroweak processes. *Phys. Lett.*, B253:161–167, 1991.

[80] Michael E. Peskin and Tatsu Takeuchi. Estimation of oblique electroweak corrections. *Phys.Rev.*, D46:381–409, 1992.

[81] M. Baak, M. Goebel, J. Haller, A. Hoecker, D. Kennedy, et al. The Electroweak Fit of the Standard Model after the Discovery of a New Boson at the LHC. 2012, 1209.2716.

[82] Marcela Carena, Ian Low, and Carlos E.M. Wagner. Implications of a Modified Higgs to Diphoton Decay Width. *JHEP*, 1208:060, 2012, 1206.1082.

[83] Aniket Joglekar, Pedro Schwaller, and Carlos E.M. Wagner. Dark Matter and Enhanced Higgs to Di-photon Rate from Vector-like Leptons. 2012, 1207.4235.

[84] Nima Arkani-Hamed, Kfir Blum, Raffaele Tito D'Agnolo, and JiJi Fan. 2:1 for Naturalness at the LHC? 2012, 1207.4482.

[85] John Kearney, Aaron Pierce, and Neal Weiner. Vectorlike Fermions and Higgs Couplings. 2012, 1207.7062.

[86] Leandro G. Almeida, Enrico Bertuzzo, Pedro A.N. Machado, and Renata Zukanovich Funchal. Does $H \to \gamma\gamma$ Taste like vanilla New Physics? 2012, 1207.5254.

[87] John F. Gunion, Howard E. Haber, Gordon L. Kane, and Sally Dawson. THE HIGGS HUNTER'S GUIDE. *Front.Phys.*, 80:1–448, 2000.

[88] Mikhail A. Shifman, A.I. Vainshtein, M.B. Voloshin, and Valentin I. Zakharov. Low-Energy Theorems for Higgs Boson Couplings to Photons. *Sov.J.Nucl.Phys.*, 30:711–716, 1979.